8-2017

On the construction and interpretation of fitness landscapes for HIV: a computational perspective

Elizabeth Grace Johnson

University of Tennessee, Knoxville, ejohns60@vols.utk.edu

To the Graduate Council:

I am submitting herewith a dissertation written by Elizabeth Grace Johnson entitled "On the construction and interpretation of fitness landscapes for HIV: a computational perspective." I have examined the final electronic copy of this dissertation for form and content and recommend that it be accepted in partial fulfillment of the requirements for the degree of Doctor of Philosophy, with a major in Microbiology.

Vitaly V. Ganusov, Major Professor

We have read this dissertation and recommend its acceptance:

Elizabeth Fozo, Suzanne Lenhart, Tim Sparer, Michael Gilchrist

Accepted for the Council:
Dixie L. Thompson

Vice Provost and Dean of the Graduate School

(Original signatures are on file with official student records.)

On the construction and interpretation of fitness landscapes for HIV: a computational perspective

A Dissertation Presented for the

Doctor of Philosophy

Degree

The University of Tennessee, Knoxville

Elizabeth Grace Johnson

August 2017

To Mom, Dad

... and the 4th floor of Hesler

(I will return all your books. I promise.)

I am indebted to the many professors, post-docs and graduate students who have contributed to my growth both professionally and personally over the course of my graduate career.

My co-advisers, Vitaly Ganusov and Michael Gilchrist, have strongly influenced my attitude towards modeling. Both have encouraged me to do the hard work of constructing practical data-driven driven models that are mechanistic in character. I have likewise been enriched by each advisor's unique perspectives on model testing and validation.

I am also grateful to Yiding Yang, a mathematician and post-doc in my lab for lending me her technical expertise and being a wonderful lab-mate who both pushed and encouraged me. Additionally, I would like to thank everyone on the 4th floor of Hesler who enthusiastically reviewed my proposals, advised me statistically, lent me books, and helped me resolve programming bugs - despite the fact that I was not in their department.

I would like to extend special thanks to committee members Liz Fozo and Dr. Lenhart for their aid and advice as I navigated my graduate career. I would also like to recognize all the experimental members of my committee who endured all manner of equations, statistics and computational jargon with extreme patience. I am also grateful to the Microbiology department, the NSF IGERT SCALE-IT, UT's SARIF program and the National Institute for Mathematical and Biological Synthesis (NIMBioS) for the financial support they provided.

“[Perfection] is the enemy of the good.”

–Orlando Pescetti

Abstract

To identify vulnerable viral targets to incorporate into an immunogen, fitness landscapes for the viral proteome have been constructed. These landscapes describe the sum or synergistic replicative cost exacted on the virus for any combination of non-synonymous mutations. Here we attempt to assess the robustness of current computational methods for measuring the fitness cost of HIV polymorphisms in these landscapes. We also address in the following chapters assumptions and shortcomings that may underlie current landscape's uneven ability to predict fitness effects.

In the first chapter, I appraise the robustness of current frame-works that derive fitness costs from patient sequence data. In this chapter I also address the fields over-reliance on cross-sectional data, justified by the assumptions that the viral populations can be 1) regarded as an ideal population at equilibrium and 2) are at large unmarred by host pressures. To explore how these problematic assumptions may undermine landscape construction, I assemble an alternate landscape, where fitness costs were directly measured from temporal population fluxes using a dynamical systems framework. This landscape paints a far different picture of the fitness topography.

In the following chapter, I tackle another problematic aspect of current landscapes, their neglect of physicochemical detail. I demonstrate that this model contrivance, leads us to under or over estimating fitness costs at positions with highly divergent or similar physicochemical character. In response, I adapt a population genetics model to account for the functional impact of each residue mutation, and illustrate that it improves our ability to predict *in vitro* viral fitness.

Finally, in the last chapter, we employ several different metrics of fitness to determine if the overall topography of the fitness landscape might shift over the course of early infection.

Research has suggested that the replicative capacity of the virus increases over time and that viral populations are continuously evolving in response to immune pressures. We found, that although the protein was not mutational static at residue resolution, at the regional and protein level it remained static due to compensating mutations.

Table of Contents

List of Tables

List of Figures

Chapter 1

Introduction

As an RNA virus, the human immunodeficiency virus (HIV) mutates at rates orders of magnitude higher than DNA based pathogens (Sanjun et al., 2010). It has been observed that HIV accumulates mutations at a rate of 1.2×10^{-5} per day per site (Zanini et al., 2016). This rapid rate of mutation allows HIV to quickly traverse and explore its sequence space, creating diverse intra-host populations within short time-frames. These diverse and mutable populations are adept at escaping the adaptive immune responses, preventing long-term adaptive immune control of the virus. (Johnston and Fauci, 2008; Walker and Burton, 2008). These same viral traits have also frustrated attempts to create an effective prophylactic vaccine, believed to be the best hope of curbing our current HIV pandemic (McElrath and Haynes, 2010; Korber et al., 2001)

Fitness landscapes can be used as a tool to predict viral evolutionary dynamics, making it easier to grasp and interpret the viruses incredible mutability and diversity. These landscapes quantitatively describe how a mutation will impair the replicative capacity of the virus given the specific genetic background the mutation is embedded in (Wright, 1932). In their simplest incarnation, computationally derived landscapes will use residue conservation at a site (the inverse Shannon entropy) as a direct proxy for fitness (Rihn et al., 2013; Ferrari et al., 2011; Liu et al., 2012). More complex models, on the other hand, will incorporate epistatic interactions between residues (Mann et al., 2014; Ferguson et al., 2013; Barton et al., 2016).

In practice, these landscapes can help predict when and where a virus will escape immune control given a patients' HLA profile (Barton et al., 2016). The highly polymorphic human leukocyte antigen (HLA) genes encode for a protein complex that presents viral peptides to the immune system. Because HLA types vary from patient to patient, particular viral peptides will elicit a strong immune response in some patients and not in others. Studies therefore often combine information from both the viral fitness landscape and a patient's HLA typing (Liu et al., 2012).

The information embedded in these fitness landscapes can also be applied to vaccine optimization problems (Ferguson et al., 2013; Shekhar et al., 2013). While it is important to create a vaccine immunogen that elicits a strong immune response, it is equally important to make sure that the virus cannot easily escape said strong immune response via accessible escape pathways (Chopera et al., 2011). Fitness landscapes can help us identify conserved elements in the viral proteome, allowing us to quantitatively describe the fragility of each conserved element and its propensity to escape immune control given its sequence background (Mann et al., 2014).

While using residue frequency as a proxy for fitness has been useful in some contexts (Ferguson et al., 2013; Mann et al., 2014), there have been notable discrepancies with computationally estimated fitness costs failing to predict a positions fragility to mutation in *in vitro* e.g. (Rihn et al., 2013) or escape rate textitin vivo e.g (Barton et al., 2016). In light of these discrepancies, we attempt to advance the field by probing the following biological assumptions made in fitness landscapes construction in the following chapters: 1) viral frequency is a robust proxy for fitness despite host pressures and small effective population size 2) ignoring physio-chemical detail in our landscapes is not skewing fitness estimates 3) that the population is at steady state.

1.1 Complications in Regard to Translating in vitro Data into Fitness Maps

Fitness landscapes are often delineated using *in vitro* methods. This is accomplished either by monitoring the growth and spread of competing for viral strains via assay or by documenting how purifying selection reshapes mutant libraries during passaging. While assays remain the gold standard for measuring fitness effects (Liu et al., 2012; Manocheewa et al., 2015), profiling a genome via passaging is regarded as a cost-effective and high-throughput alternative.

There are two commonly employed fitness assays, growth competition assays and spreading replication assays. In growth competition assays, the growth ratio between a mutated genotype and a wild genotype is used do quantify the fitness impact of a mutation (Hinkley et al., 2011; Holland et al., 1991). In spreading replication assays, however, it is the number of infected cells that are used as a proxy for fitness (Rihn et al., 2013). In these assays, a fluorescent protein is often inserted into the proviral template, allowing the infection ratios to be calculated by FACS analysis. These described assays for viral fitness, while accurate, are expensive, labor intensive and also fail to detect small fitness effects, where replication costs drop below 5 percent. (Zanini et al., 2016). Therefore, they remain unrealistic approaches for uncovering multidimensional fitness maps, which require high coverage.

In contrast to assays, recently developed high-throughput approaches (Thyagarajan and Bloom, 2014; Wu et al., 2014; Al-Mawsawi et al., 2014; Acevedo et al., 2014) seem more suited to uncovering fitness landscapes, because they are sensitive, less labour intensive and more cost effective. These methods require the initial construction of a plasmid mutant library of the region of interest. These libraries are often created using low fidelity PCR approaches. These plasmid libraries are then transfected into cell cultures where the produced virus undergoes multiple subsequent passages in cell/tissue culture. Deep sequencing can them be employed to quantify the frequency or resulting amino acid preference at each site in the passaged population. By observing the frequency of residue mutations present before and after the purifying selection, a value called the Relative Fitness can be calculated. This value is the ratio of a genotype frequency post-passaging to a mutational frequency pre-passaging. While this approach seems

Table 1.1: Notable in-vitro derived fitness landscapes for RNA viruses Bellow are shown several different empirical landscapes from the literature derived from growth assays where stock or patient derived virus is competed in culture.

growth and activity assays

Author	Virus (Region)	Assay
(Rihn et al., 2013)	HIV-1 (CA)	spreading infection assay
(Hinkley et al., 2011)	HIV-1 (RT) (PR)	growth competition assay
(Petropoulos et al., 2000)	HIV-1 (RT) (PR)	luciferase activity assay
(Parera et al., 2007)	HIV-1 (PR)	growth competition assay

passage of mutant libraries

Author	Virus (Region)	Passage
(Thyagarajan and Bloom, 2014)	Inf(HA)	MDCK-SIAT1 cells
(Wu et al., 2014)	Inf (HA)	A549 cells
(Al-Mawsawi et al., 2014)	HIV-1	293T cells
(Acevedo et al., 2014)	Poliovirus	Human diploid fibroblasts

more tractable for constructing fitness landscapes, detailed profiles of Influenza's HA protein conducted on two different cell lines do not seem to agree (Thyagarajan and Bloom, 2014; Wu et al., 2014), suggesting that this method might produce very different landscapes depending on how the virus is passaged.

1.2 Current Computational Approaches to Calculating Fitness Costs and Constructing Fitness Landscapes

A range of techniques have been adopted and devised to estimate fitness costs from patient data. These techniques can be as simple as a Shannon entropy derivation or as computationally intensive as fitting a Potts models to a whole protein (Barton et al., 2016). However, one unifying aspect of almost all of these techniques is that they are dependent on cross-sectional sequence data for model inference (Table 1.2). This dependence has its pitfalls, as it ignores possible footprints left in sequences data host immune pressures. Concerned that these footprints might be misinterpreted as intrinsic fitness pressures, (Zanini et al., 2016) has instead constructed a fitness landscape informed by longitudinal sequences.

Shannon Entropy is a metric used across diverse fields to describe information content. In this particular context, it is best conceived of as our ability to predict the correct residue at a position given a sequence randomly drawn from the viral population. High Shannon entropy indicates that one would likely have to guess many times before correctly naming the right amino acid. Positions like these are regarded as robust to mutation. Low Shannon entropy positions, on the other hand, would require fewer guesses and would be regarded as under strong purifying selection. A position's Shannon entropy can predict how rapidly it will mutate to escape immune detection (Ferrari et al., 2011; Allen et al., 2005; Li et al., 2007; Liu et al., 2012) and correlates well with sequence conservation. Because of this, Shannon entropy is often employed as a surrogate measure for fitness (Liu et al., 2012; Fernandes et al., 2016). However it will sometimes over or under predict fitness effects as noted by (Rihn et al., 2013; Barton et al., 2016).

Table 1.2: Models used to Infer Fitness Landscapes Shown below are computational landscapes used to infer fitness in the HIV literature. All but one is derived from cross-sectional sequence samples.

Cross-Sectional Data

Author	Model Description
(Dahirel et al., 2011)	Principle Component Analysis and Random Matrix Theory (RMT)
(Ferguson et al., 2013)	Ising Model
(Mann et al., 2014)	Ising Model
(Barton et al., 2016)	Potts Model and Wright-Fisher Simulation

Longitudinal Data

Author	Model Description
(Zanini et al., 2016)	mutation selection balance model curve fit

Colinkage or epistasis across the Gag-polyprotein fitness landscape has been investigated by (Dahirel et al., 2011) in a principal component analysis of a similarity matrix of Gag polyprotein sequences. Using this analysis, residue sectors or groups that evolved together were able to be identified. Random matrix theory (RMT) was used to distinguish noise from real multi-dimensional constraints. The correlation matrices themselves were constructed from cross-sectional sequences samples. Results demonstrated that the genome is heavily co-linked and five separate sectors of co-evolving residues were identified.

While principle component analysis can extract higher order relationships between residues, Potts and Ising models can extract both fitness costs and epistasis. The Potts model is a model from statistical physics used to characterize the change in a systems energy and entropy due to collective interactions. In the Potts model, each sequence number k is treated as a vector $\vec{z}^{\,k}$ containing either interacting binary variables $(1, 0)$ to represent mutant and wild residues in the simplified Ising model or a full set of interacting amino acids in the Potts model. The value $P(\vec{z}^{\,k})$ represent the probability of observing a sequence number k. The probability $P(\vec{z}^{\,k})$ represents the probability of observing sequence number k given how likely each residue is by itself $h_i(z_i^k)$ and how likely each residue pairings is $J_i(z_i^k, z_j^k)$.

$$P(\vec{z}^{\,k}) = \frac{1}{Z} e^{-E(\vec{z}^{\,k})} \tag{1.1}$$

$$E(\vec{z}^{\,k}) = \sum_{i}^{m} h_i(z_i^k) + \sum_{i}^{m} \sum_{j=i+1}^{m} J_i(z_i^k, z_j^k) \tag{1.2}$$

This term J, therefore, is able to accounts for synergistic and antagonistic interactions between sites. In this way, we can think of $E(\vec{z}^{\,k})$ as the Hamiltonian in our equation giving us an entropy value for our particular sequence. As this entropy value gets large (as the sequence becomes more unlikely), the entropy increases and our probability of observing that sequence decays 1.1. The decay term is scaled by a partitioned function Z giving us the probability of k relative to the probabilities of the other sequences. These hi and Jij entropy mappings can be fit to sequence data, and can then be used to calculate the relative fitness of a sequence.

Both (Mann et al., 2014) and (Ferguson et al., 2013) have adapted Ising models to extract fitness landscapes from sequence data to great success for the Gag protein. However, these models require each sequence to be compressed into to a bit-string, which is only an appropriate for highly conserved proteins. (Ferguson et al., 2013; Shekhar et al., 2013). As a result, these models have limited application and cannot predict fitness costs in immunologically crucial regions such as the envelope. Efforts have been made to run adapt a full Potts model for fitness cost extraction (Barton et al., 2016). The computation obstacles inherit in this approach proved to be intractable, and the residue diversity had to be compressed for most positions along the proteome. The resulting fitness metrics also failed to robustly predict escapes with out the aid of outside data.

There has been only one case of a model using longitudinal patient data for its fitness landscape inference. In this unpublished work, (Zanini et al., 2016) has used whole genome deep sequencing data from 9 patients sampled 6 to 12 times over the course of an early infection. From this data, saturation trajectories of various single nucleotide polymorphisms are recorded and a mutation selection balanced saturation function 1.3 is fit to the SNP temporal dynamics. From this fit, the author is able to obtain selection coefficients against the various SNPs. Using these selection coefficients he constructs a map of the HIV genome with more than 50% percent coverage.

$$\langle x \rangle = \frac{\mu}{s}(1 - e^{-st}) \tag{1.3}$$

A function above (Eq.1.3) is used to describe the average trajectory of a single nucleotide polymorphism (SNP). In this function μ stands for the mutation rate s for the fitness cost or selection coefficient and t for time. In this function, the SNP frequency will saturate as time goes on. Because mutations tend to be transitory or only semi-dominant in the population (Novitsky et al., 2009) the SNPs trajectories taken from the data were exceedingly noisy (Zanini et al., 2016). Due to this noise, extraction of selection coefficients was non-trivial. The process required both extensive trajectory smoothing and averaging among patients.

1.3 Addressing Assumptions and Weaknesses in the Current Computational Approaches

One concern with computationally generated landscapes is their over-reliance on cross-sectional data (Mann et al., 2014; Ferguson et al., 2013; Barton et al., 2016). These cross-sectional sequences are used to calculate the frequency of mutation in particular regions. However it is not clear if mutations are enriched in a region because 1) that region is more structural and functionally permissive to mutation, 2) or because this region has undergone multiple selective sweeps by the immune system and therefore has been enriched with mutations (Zanini et al., 2016). To address this problem, we used longitudinal data of early infections to observe rate of fixation of viral mutations as an alternative method to obtain fitness costs. Here we attempt to assess the robustness of current methods for measuring the fitness cost of HIV polymorphisms.

Another problematic aspect of current landscapes is that they ignore the physicochemical nature of the residues composing the map (Mann et al., 2014). Each residue is regarded as interchangeable with the next in terms of size, polarity and side-chain composition. In such cases we may be under estimating fitness costs at positions hosting a diversity of residues that are physicochemically uniform. Conversely, we may also be over estimating fitness costs at positions hosting a few residues that are physicochemically divergent. From a database of HIV sequences, we may observe that a particular position hosts a diverse set of residues. At first glance, this diversity might suggest there is not a great deal of purifying pressure exerted on that position. However, upon further examination, we may find that the residues at this site tend to be quite physiochemically similar. This conservation of physiochemical characteristics alternatively suggests that a high degree of purifying pressure is exerted on that position. Conversely, a position may be fairly non-diverse in its residue variety; but the residues may be quite physiochemically distinct from one another. In this situation, purifying pressure may exert much less force on that position than one might assume from residue diversity alone.

Finally, because fitness landscapes are usually not derived from longitudinal data, it is not clear if the fitness landscape is dynamic or static over the course of infection. By dynamic we mean shifting in distance from the consensus virus over infection, and fundamentally changing its character as it adapts to the host. Previous work examining *ex vivo* fitness of longitudinally sampled patient virus has show that the replicative capacity of the virus seems to increase over time (Quiones-Mateu et al., 2000; Troyer et al., 2005). This would seem to suggest the fitness landscape is organizing itself around the consensus viral sequence. This fitness however is measured using an exogenous replication system that does not recapitulate the host environment with its cytokines and immune factors, in addition others have found viral replication capacity to decrease over time in the presence of adaptive immune pressures (Arnott et al., 2010). Given that Gag-poly protein is one of the main structural poly-proteins in the virus and the most conserved (Li et al., 2013), we wanted to know how it evolved in regard to the consensus sequence over time. Evidence from longitudinal data (Novitsky et al., 2009) seemed to suggest that the protein was dominated by mutational reversion that went to fixation during early infection and by transient forward mutations away from fit consensus residues later in infection.

Chapter 2

Discordance of HIV fitness-landscapes created using cross-sectional vs longitudinal data

Abstract

HIV is a genetically plastic virus, adept at evading the patient's adaptive immune system. The virus avoids immune recognition by mutating key residues embedded in epitopes targeted by adaptive responses. However, these substituted residues can be structurally and functionally suboptimal for the virus. Fitness landscapes of the virus quantitatively describe, with residue level resolution, the particular cost exacted on the intrinsic fitness of the virus for these mutations. In computationally derived landscapes, residue frequency is regarded as the underlying signature of fitness. The more fit an amino acid residue is the more often one would expect to observe it at that particular position. We compared the robustness of methods using cross-sectional data against each other and a fitness map extracted from longitudinal data. The temporal resolution of the longitudinal data sets enables us to estimate fitness cost from viral population kinetics within an individual patient. In this analysis of fitness, compartmentalization of replication and inter-patient variation is perhaps less of a confounding factor. We find significant discrepancies between the fitness maps derived from cross-sectional patient data and the map derived from longitudinal data. The lack of concordance suggests that they are perhaps not actually measuring the same phenomenon.

2.1 Introduction

2.1.1 Fitness Landscapes and HIV Diversity

HIV is a highly mutable and diverse virus. This inherit mutability and diversity have stymied efforts to create the vaccine immunogens necessary to curb the ongoing pandemic. An estimated 70 million people have been infected with the retrovirus since the start of the pandemic, with 1.1 million dying from an AIDS associated illness in 2015 alone and 2.1 million new infections detected in the same year Global Aids Response Progress Reporting (GARPR, 2016). It has been proposed that an effective vaccine immunogen should not only elicit strong responses against highly conserved residues but also against residues that are marginally costly for the virus to mutate (Walker and Burton, 2008; Troyer et al., 2009). Residues that are costly to mutate are said to have "high fitness costs" in that they exact a high price on viral replication. A position may not be entirely deleterious to mutate but can be costly enough that it impairs the replicative capacity of the virus. It has been shown that individuals who control the virus possess virus that replicates poorly (Miura et al., 2010). In particular strong immune recognition of Gag epitopes correlates well with lower viral loads during the later stage of chronic infection (Sunshine et al., 2015). Fitness landscapes of conserved proteins like Gag, help us identify which particular positions we want to elicit immune responses against if we wish to accrue costly mutations in the viral population. By accruing expensive mutations, one can push the virus towards its error threshold. These landscapes also reveal the hyper-conserved regions where there is little to no deviation from the consensus sequence either due to strong intrinsic purifying pressures, or the lack of any notable external selective pressures.

2.1.2 Methods for deriving fitness landscapes from cross-sectional data

Shannon Entropy calculations (Rihn et al., 2013; Liu et al., 2012; Ferrari et al., 2011) and Entropy Maximization models (Ferguson et al., 2013; Mann et al., 2014; Shekhar et al., 2013) have both been used to gauge fitness costs associated with escape mutations and estimate escape times from immune responses. When employing either method, it is assumed that sequences are sampled from a putatively large and rapidly mutating RNA virus population can be treated as a homogenous idealized population at equilibrium. In these idealized populations, the frequency landscape for HIV polymorphisms is treated as a direct proxy of the fitness landscape for these polymorphisms (Shekhar et al., 2013). Cross-sectional patient data is pooled together to produce these prevalence landscapes.

The degree to which natural intra-host HIV populations actually resemble a homogeneous ideal population at equilibrium is unclear. While the census size population for HIV is quite large (10^8-10^7) the effective population size may be quite small (10^4) (Shriner et al., 2004; Rouzine and Weinberger, 2013). Also, notably, the HIV population is never at true equilibrium, but is continually perturbed by host selective pressures and is constantly in flux. (Holmes and Moya, 2002),(Hedskog et al., 2010)(Tsibris et al., 2009). Yet more concerning, the viral population is heavily compartmentalized spatially in the secondary lymphoid tissues (van Marle et al., 2007) (Rozera et al., 2014) (Sturdevant et al., 2015) and seems unlikely to behave as a homogeneous unit.

The second simplifying assumption the Shannon entropy calculation and maximum entropy model share, is residue interchangeability. Each residue, regardless of its physio-chemical properties is distinguished (at most) as either consensus or non consensus. However, the fitness of a mutation does seem to be residue specific in HIV, with residues with similar R groups tending to more readily replace each other (Grantham, 1974).

2.1.3 Deriving Fitness Landscapes using intra-host dynamics (Longitudinal Data)

Gauging fitness costs from longitudinal patient data, in contrast, does not require one to assume the viral sequences were taken from large idealized population at equilibrium. Instead of using frequency as a proxy of fitness, the rate of fixation in the population is used as an estimate of fitness (Davenport et al., 2008). Using differential equations that account for growth differentials and immune pressure, one can get a more precise estimation of the fitness difference (eq. 2.14), (Ganusov and De Boer, 2006; Fernandez et al., 2005). By applying this dynamical system approach on a position by position basis, we will show it is possible to construct a fitness cost map for a section of the HIV genome.

2.1.4 Deriving Fitness Landscapes using physio-chemical properties of residues (Cross-sectional Data)

On cross-sectional Multiple Sequence Alignment data (MSA), we used a more complex incarnation of the Maximum Entropy model adapted from work done by Shah and Gilchrist.(Shah and Gilchrist, 2011; Gilchrist, 2007; Gilchrist et al., 2009). In this formulation, all mutations are not treated as equally deleterious to the virus. Instead, the functional impact of each mutation is taken into account. To achieve this, a physio-chemical distance measurement is employed to gauge how different a mutant residue is from the putatively optimal residue. Physio-chemical attributes considered in the distance measurement includes properties such as polarity, charge, and size (Grantham, 1974).

2.2 Methods

2.2.1 Cross-sectional Sequences

We use 1058 curated sequences in the Los Alamos database for subtype C (2016) . These sequences were filtered web alignments that provide a good example of the subtypes breadth. Every sequence belongs to a unique patient and sequences that resemble each other too closely had been removed. Additionally questionable sequences such as those that appear to be hyper-mutants and synthetics have also been removed. The curated sequences were clean, containing little ambiguous coding, few long insertions and lacked a preponderance of frame shifts. Sequences in this curated alignment were aligned using both automation (HMMER) and manual editing.

2.2.2 Longitudnal Sequences

The HIV-1 Gag sequences used to construct the viral population kinetics in this analysis, came from a primary HIV-1 subtype C infection study conducted in Botswana from 2004-2005 (Novitsky et al., 2009). In this study, a cohort of 42 HIV-1 subtype C positive individuals had their blood drawn at 4-6 points in a 500 day period after sero-converting. Patients were newly infected. Of the 42 patients, 34 individuals were in Fiebig stage IV or V (20-100 days post infection) the other 8 were still in Feibig II (˜15-20 days post infection). The accession numbers for the sequences are as follows: GQ275380–GQ277569, GQ375107–GQ375128, GQ870874–GQ871183. It was impossible to get a linear fit for Patient "OM" individually because the patient had only two recorded blood samples. Therefore patient "OM" is omitted from the sample in the patient breakdowns.

2.2.3 Generating Confidence Intervals for the Longitudinal Patient Samples

The data points we fit in the models were binomial proportions as viral strains were categorized in a binary fashion as either consensus or non-consensus. Because the number of samples per time point was small n=(5-30) we elected to use a Jeffery's prior interval (Jeffreys, 1946) to calculate the confidence intervals around the frequency of the wild-type at each timepoint. The Jeffreys interval is derived from the Binomial Distribution using Bayes Theorem and Jeffery's Prior (Brown et al., 2001). This interval uses a Beta distribution $I(\alpha, \beta)$ with shape parameters $\alpha = 1/2$ and $\beta = 1/2$ as a prior probability density function:

$$\text{Prior: } I_x(1/2, 1/2) \tag{2.1}$$

The shape parameters are then updated with more information about the data. If we find $\hat{x}$ consensus viral residues out of n total residues we adjust the probability density function as follows:

$$\text{Posterior: } I_x(\hat{x}+1/2, n-\hat{x}+1/2) \tag{2.2}$$

The confidence interval can then be written as the quantile below:

When $\hat{x} \neq 0$ and $\hat{x} \neq 1$:

$$\text{upper CI: } I^{-1}_{\frac{1-\alpha}{2}}(\hat{x}+1/2, n-\hat{x}+1/2) \tag{2.3}$$

$$\text{lower CI: } I^{-1}_{\frac{\alpha-1}{2}+1}(\hat{x}+1/2, n-\hat{x}+1/2) \tag{2.4}$$

Boundary Cases: As the frequency tends to zero or one, we lose coverage using this distribution. Therefore for borderline cases when $\hat{x} = 0$ we set the the lower limit equal to zero and when $\hat{x} = n$ we set the upper limit equal to 1 (Brown et al., 2001).

2.2.4 Mathematical Models

Four different approaches for creating fitness landscapes are detailed (Fig. 2.1) each using a different metric as a surrogate for fitness. The Shannon Entropy Metric, Maximum Entropy Metric, and the PhysioChemical Metric are estimated or calculated using the same cross-sectional set of sequences. The Ordinary Differential Equation fitness metrics,however, are estimated using longitudnally sampled set of sequences. These models do not account for epistasis between positions, but can be extended to do so.

Model A: Shannon Entropy Metric

$$w_{ij} \propto \frac{x_{ij}}{N} \tag{2.5}$$

$$p_{ij} = \frac{w_{ij}}{\sum\limits_{j=1}^{20} w_{ij}} = \frac{x_{ij}}{N} \tag{2.6}$$

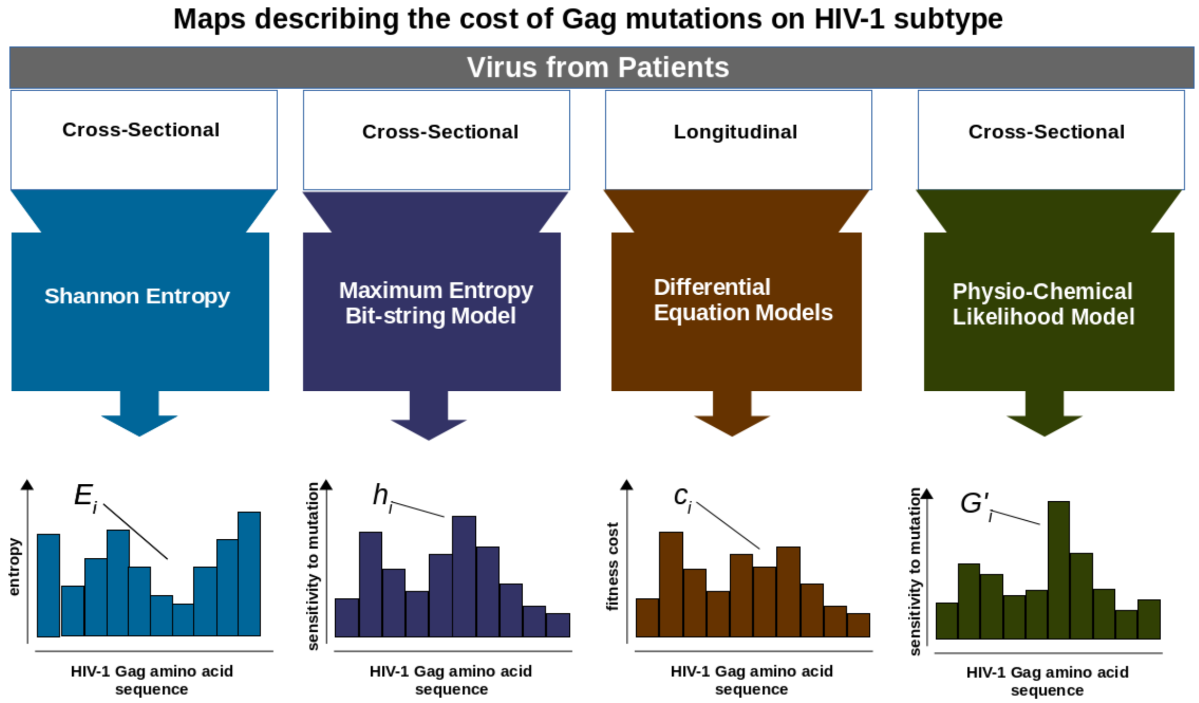
Maps describing the cost of Gag mutations on HIV-1 subtype
Virus from Patients
Cross-Sectional
Cross-Sectional
Longitudinal
Cross-Sectional
Shannon Entropy
Maximum Entropy Bit-string Model
Differential Equation Models
Physio-Chemical Likelihood Model
entropy
E_i
HIV-1 Gag amino acid sequence
sensitivity to mutation
h_i
HIV-1 Gag amino acid sequence
fitness cost
c_i
HIV-1 Gag amino acid sequence
sensitivity to mutation
G'_i
HIV-1 Gag amino acid sequence

Figure 2.1: Summary of landscapes used to assess concordance Shannon Entropy (E_i): Mutational cost estimated from diversity of amino acids at the position. Maximum Entropy (hi): Mutational cost estimated from the number of deviations from consensus tolerated by the position. Differential Equation Models (c_i): Mutational cost estimated from the rate of fixation of non-mutated positions. Physio-Chemical Likelihood Model (G'_i): Mutational cost estimated by observing the variety and degree of physio-chemical deviations tolerated by the position.

$$E_i(X) = -\sum_{j=1}^{20} p_{ij} \ln p_{ij} \tag{2.7}$$

The term x_{ij} is the number of residues j observed at position i in the cross-sectional sample of sequences. The fitness w_{ij} of any particular amino acid residue j at position i is proportional to the number of residues j observed at that position (x_{ij}) divided by the total number of residues observed N. We can then write the probability p_{ij} of observing each of the residue's given the residues proportional relative fitness compared to the total relative fitness of the other residues. The entropy of the position defined by those probabilities E_i is defined by equation 2.7.

Model B: Maximum Entropy Model

In an entropy maximization framework, the population is organized around one well defined master sequence. This master sequence, or consensus, represents a hypothetical "most fit" version of the virus. All deviations from a position in the master sequence are treated as equally deleterious for the virus. The below model is a single position simplification of the Ising maximum entropy model presented by (Ferguson et al., 2013),(Mann et al., 2014),(Shekhar et al., 2013). In this model, h_i in the sensitivity of that position i in the sequence to mutation.

$$w_{ij} \propto \exp[-h_i \cdot d_{1,0}(a_{i,j})] \tag{2.8}$$

$$p_{ij} = \frac{w_{ij}}{\sum\limits_{j=1}^{20} w_{ij}} \tag{2.9}$$

$$p_{i,j=c_i} = \frac{1}{19 \cdot e^{-h_i} + 1} \tag{2.10}$$

$$p_{i,j \neq c_i} = \frac{e^{-h_i}}{19 \cdot e^{-h_i} + 1} \tag{2.11}$$

$$\mathcal{L}(h_i|X) = \frac{\Gamma(\sum_j x_{ij} + 1)}{\prod_j \Gamma(x_{ij} + 1)} \prod_{j=1}^{20} p_{ij}^{x_{ij}} \tag{2.12}$$

The relative fitness (w_{ij}) of variants bearing amino acid j at position i is proportional to an exponential term that decays depending on the distance $d_{1,0}$ of the amino acid j from the putative optimal and the degree of sensitivity of the position h_i to mutation. The distance term $d_{1,0}$ is defined by astep function function where $d_{1,0}(a_{ij}) = 1$ if the amino acid is not the consensus residue and $d_{1,0}(a_{ij}) = 0$ if the residue is the consensus residue. We can then write the probability p_{ij} of observing each residue, given the residues proportional relative fitness compared to the total relative fitness of the other residues. There will be one probability for non-consensus residues $j \neq c_i$ and another for consenus residues $j = c_i$. Using a maximum likelihood estimation we can then estimate what sensitivity h_i is most likely for that position given the frequency distribution of amino acids (X) observed at that position.

Dynamical Systems Model C: Differential Equation System

By applying this differential equation system on a position by position basis, a cost map for a section of the genome can be constructed. The parameter c in this model is the replication penalty exacted on a position i carrying a mutation.

Below, is a set of closed form equations describing how the number of viral variants change over time within a patient. The closed form equations were derived from a set of differential equations one representing the change in the consensus and non-consensus variants over time with and without an effector response. The closed form solution, describes how the frequency of the wild variant may shift over time, given its initial starting frequency f_0 and the degree c to which the mutant variant's replication is impaired (Fig 2.2).

$$f_w(t) = \frac{f_0}{(1 - f_0)e^{-crt} + f_0}, \tag{2.13}$$

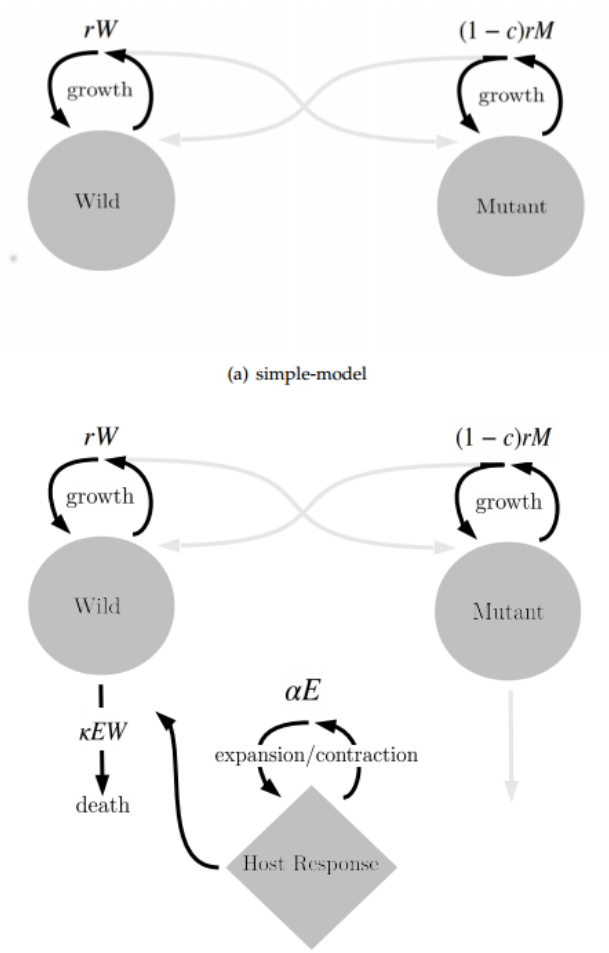

(a) simple-model

(b) immune-model

Figure 2.2: ODE models to extract fitness costs Models employed to extract fitness cost estimates for reverting positions.**A.** The first model assumes no immune response against the reverting position **B.** The second model includes immune pressure targeted against the consensus variant

$$
\begin{aligned}
f_w(t) &= \frac{f_0 e^{\frac{\lambda}{\alpha}}}{(1-f_0)e^{\frac{\lambda e^{\alpha t}}{\alpha}-crt} + f_0 e^{\frac{\lambda}{\alpha}}}, \\
\lambda &= \kappa E_0.
\end{aligned}
\tag{2.14}
$$

Table 2.1: Table of State Variables and Parameters for ODE Models The following state variables and parameters are shared between the ordinary differential equation models.

parameters	
f_w	frequency of wild variant
f_0	initial frequency of wild variant
μ_w	mutation rate of wild into mutant population
μ_m	mutation rate of mutant into wild population
c	replicative cost of mutation
r	growth constant of wild variant
κ	killing rate of effector cells
α	expansion rate of effector cells
E_0	initial population of effector cells
state variables	
M	RNA copies of mutant variant per ml of blood
W	RNA copies of wild variant per ml blood
E	effector response of immune system

A likelihood ratio test was used to compare how well the simple reversion model and the immune-reversion model fit the same data set. This statistical test requires that one of the models be a nested version of the other. It can be easily shown that our simple reversion model is a nested version of the more complex immune model. The complex immune model can be converted into the simple model by constraining the clearance rate κ by setting it equal to 0.

The parameters f_0,c,α and λ were estimated using a binomial log likelihood fitting of the data. In this binomial log likelihood fitting, we identified an optimal set of parameters that described the observed residue frequencies at the different time points given the underlying binomial distribution of the sampled data. The sampling of the virus was bernoulli like, and there was also a significant discrepancy in sample number between the timepoints. Therefore, this binomial log likelihood fitting procedure described above was preferable to a least squares fitting procedure. The combination of parameters that produced the most probable frequencies given the data and model were identified numerically using a downhill simplex algorithm (Nelder-Mead) and a constrained optimization by linear approximation (COBYLA). The objective function used in this non-linear minimization is given below (eq. 2.15):

$$\ln(\mathcal{L}(\theta;X)) = \sum_{i}^{N} \ln\left(\binom{n_i}{x_i} f_w(\theta,t_i)^{x_i}(1-f_w(\theta,t_i))^{n-x_i}\right) \tag{2.15}$$

The parameter θ is the vector of model parameters: f_0,c,α and λ. The data term X is the presence/absence data for the consensus residue at different timepoints in the patient. The number n_i is the number of viral sequences amplified at timepoint i while x_i is the number of viral sequences amplified at timepoint i bearing a consensus residue at the position. The value f_w is the estimated frequency of consensus residue as predicted by the model. The value t_i denotes how many days post-seroconversion the patient is at sample i with N representing the total number of samples during the infection.

Estimating fitness cost for rapid reversions and generating parameter confidence intervals

Reversions in Gag often happen rapidly (within 100 days or less) (Novitsky et al., 2011) and the temporal resolution in this study is somewhat low with an average of 6 samples per 500 days. As a result, a reversion will often occur between two sampling periods. Since the frequency jumps from 0 to 1, it is difficult to determine the fitness cost that drove the rapid reversion given the logistic behavior of our model. This difficulty is addressed by re-sampling the data assuming a continuous beta distribution (the conjugate prior probability distribution for the binomial distribution) underlies the data, refitting the re-sampled data and thereby obtaining a distribution of possible c-values. The median of these c-values is then taken as our best guess for c (Fig 2.3).

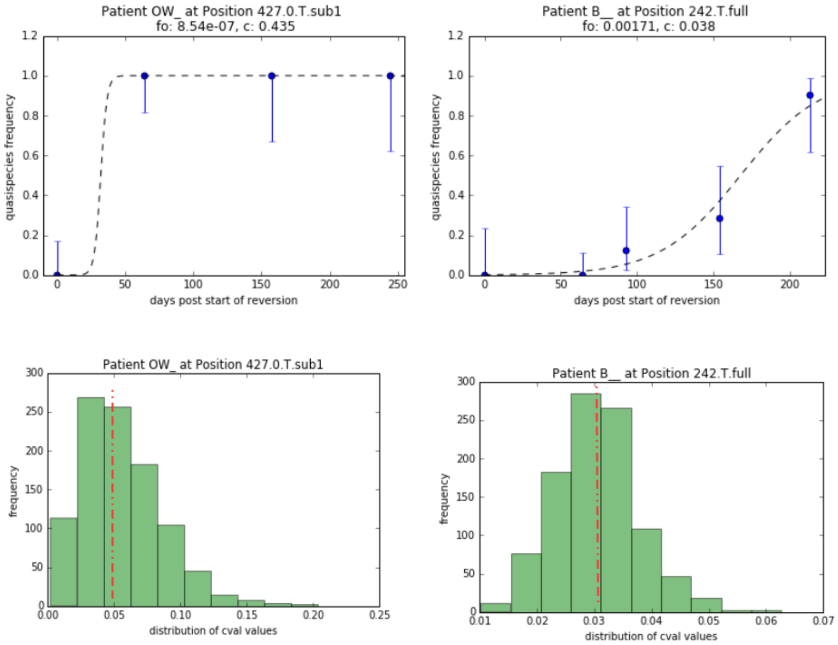

Figure 2.3: Bootstrapping Example of resampling at position 427 and 242 in two patients experiencing a viral reversion back to the consensus residue over 250 days. The samples at each time-point were bootstrapped 1000 times, creating 1000 new reverting trajectories. the distributions of the data and refitting the data produces a distribution of 1000 cost values for each position.

2.3 Results and Discussion

The fitness map generated from reversion kinetics did not strongly correlating with fitness maps generated from Ising or physiochemical measures of sensitivity to mutation (Fig. 2.4)

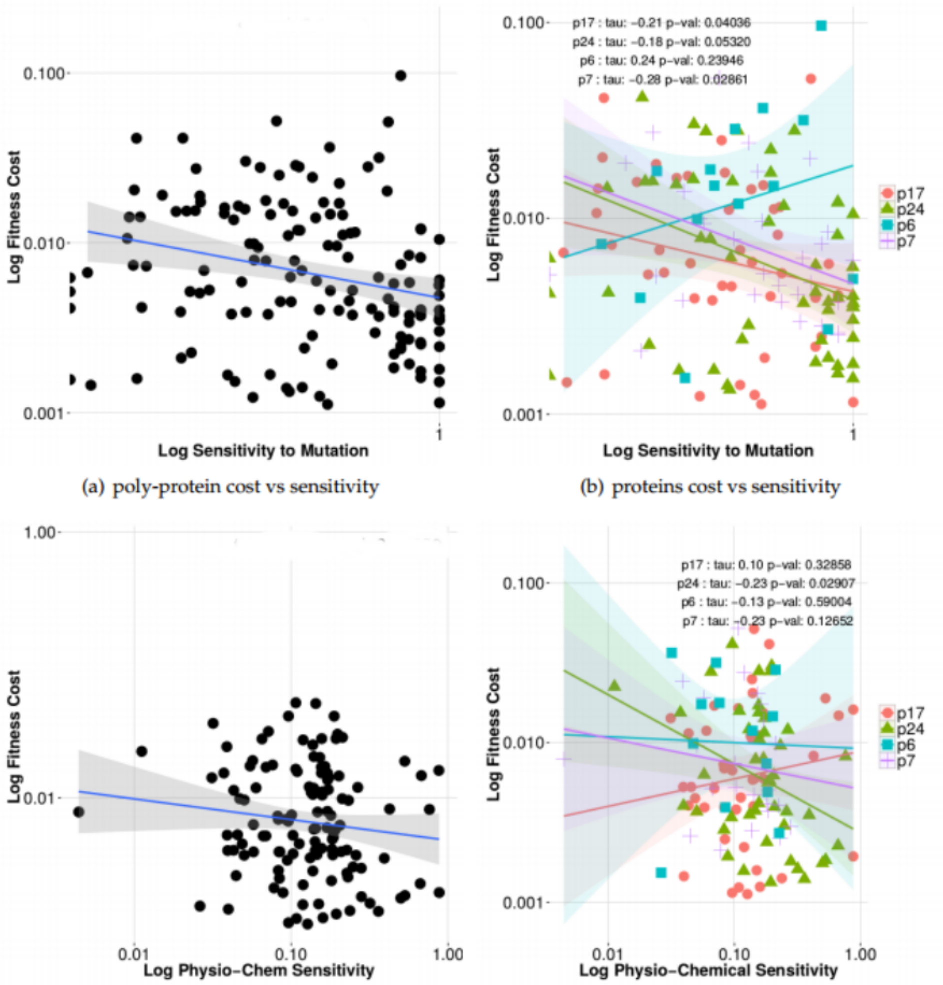

(a) poly-protein cost vs sensitivity

(b) proteins cost vs sensitivity

(c) poly-protein cost vs phys-chem sensitivity

(d) proteins cost vs phys-chem sensitivity

Figure 2.4: Correlation between non-standard metric Absence of a strong negative correlation between the simplified Ising / Physio-Chemical sensitivities and fitness cost (τ=-0.18 ns and τ=-0.09 ns) for full protein respectively. Points represent HXB2 position coordinates for which there was a reversion from which a fitness cost could be extracted. On the x-axis we plot that HXB2 positions corresponding sensitivity to mutation from cross-sectional sequences. On the y-axis we plot the HXB2 positions corresponding fitness cost as extracted from the longitudinal sequences. The concordances are displayed for all HXB2 positions along the poly-protein **(A and C)** and per protein **(B and D)**.

However the fitness map generated from reversion kinetics did negatively correlate at both the poly-protein and protein level with Shannon entropy calculations (Fig 2.5) This negative concordance was unexpected. However, these results seem to be

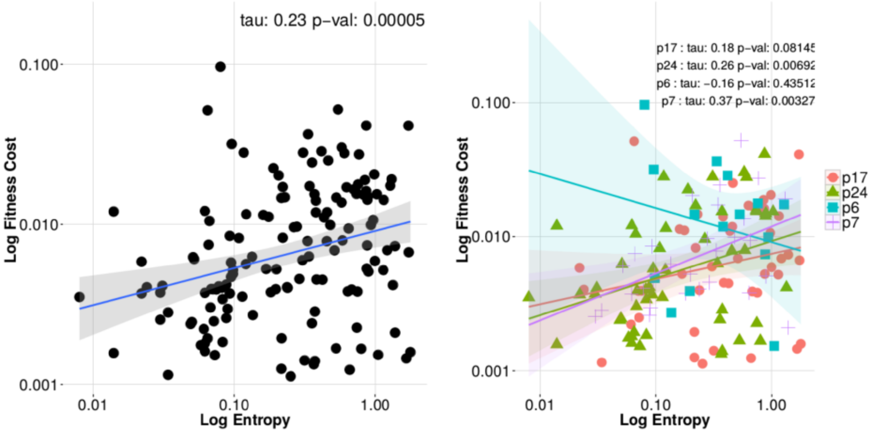

(a) poly-protein cost vs entropy

(b) proteins cost vs entropy

Figure 2.5: Correlation with Entropy S ignificant positive correlation between entropy and fitness cost using a kendall tau concordance statistic Points represent HXB2 position coordinates for which there was a reversion from which a fitness cost could be extracted. On the x-axis we plot that HXB2 positions corresponding entropy from cross-sectional sequences. On the y-axis we plot the HXB2 positions corresponding fitness cost as extracted from the longitudinal sequences. The concordances are displayed for all HXB2 positions along the poly-protein **(A)** and per protein **(B)**

robust, even under conservative assumptions where only classical reversions are used for the analysis. By classically reverting, it is meant that the fitness cost value extracted from the reverting positions was subset out of the analysis if the confidence intervals of the cost value c overlapped with 0. Out of the 862 reverting position only 115 met this criteria. Values displayed on the fitness maps represent the maximum fitness cost calculated for that position. Fitness values for positions displayed on the concordance plots represent an average of c-values for this position. Position had anywhere from only one estimate of c for each position to as many as 8 estimates over the patients (Fig 2.6).

We see in Figure 2.4 that the estimates of mutational sensitivity extracted from cross-sectional data are poor correlates of fitness cost as estimated from

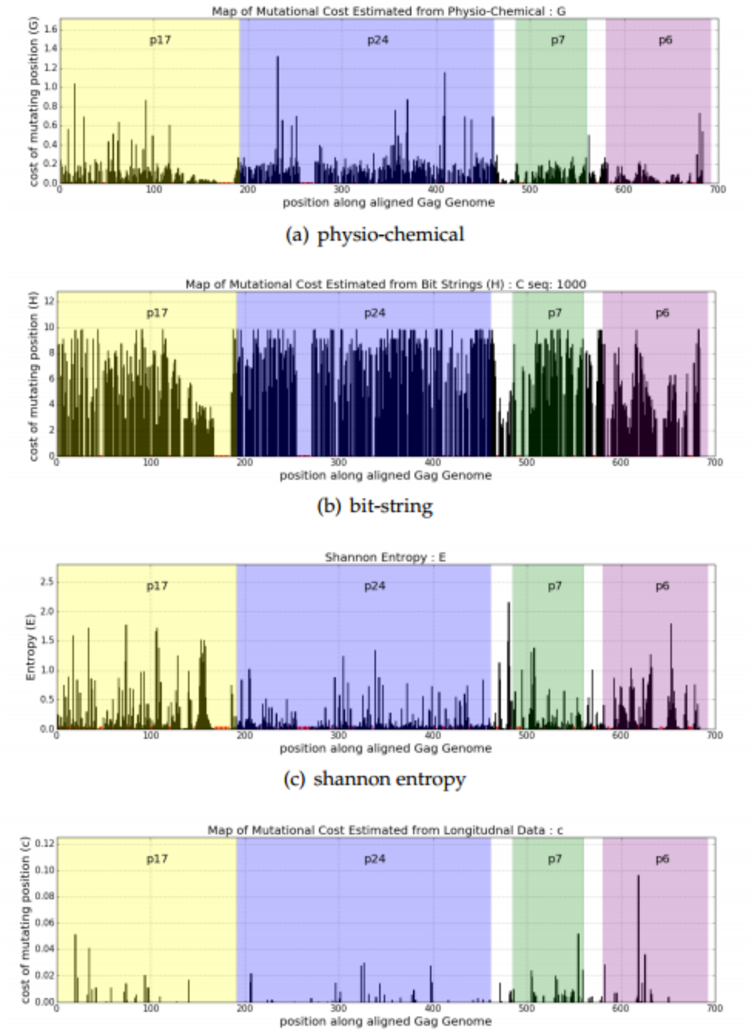

(a) physio-chemical

(b) bit-string

(c) shannon entropy

(d) ODE Model

Figure 2.6: Bar Plot of Metrics The x-axis on each plot denotes our location along the set of 1000 aligned Gag-polyprotein. The y axis describes the fitness cost (c,H,G') or entropy (E) associated with each location. The Gag poly-protein encoded by these sequences is broken down into functional units by color on the plot. These units include p17 the matrix, p24 the capsid, p7 the nucleocapsid and p6 the nucleoprotein. **(A)** The fitness cost unit G is a measure of how fragile a position is to deviations from consensus. It estimates this fragility by observing how the position tolerates physio-chemical deviations from the consensus residue. **(B)** The fitness cost unit H is also a measure of how fragile a position is to deviations from consensus. However,it uses a purely binary metric of deviation without any physio-chemical detail. **(C)** The entropy measure E is the Shannon Entropy of each position. The Shannon Entropy is a measure of residue diversity regarded as an inverse proxy of fitness cost in the literature. **(D)** The fitness cost c describes to what degree the replication capacity of the virus has been reduced if there is a mutant residue at that position

reversions. Shannon entropy, in contrast, has a significant positive correlation with fitness cost (Fig. 2.4), precisely the opposite of what one would predict. One would expect that a hyper variable position would not be costly to mutate and we would see slow reversions at that position. Conversely, one would expect a conserved position to revert to consensus rapidly. However, we observe the opposite. It is the variable positions (high entropy positions) that revert rapidly and it is the non-variable/conserved (low entropy positions) that revert slowly.

2.3.1 Shannon Entropy as proxy for fitness cost: considerations

Either Shannon entropy is a poor proxy for fitness, reversion rate is a poor proxy of fitness, or both poorly measure fitness. There is evidence that Shannon entropy can sometimes fail to predict fitness well in competition assays (Rihn et al., 2013) and is not necessarily a robust measure of viral escape time from the immune response (Barton et al., 2015). The replication of the virus is believed to be somewhat compartmentalized (van Marle et al., 2007) (Rozera et al., 2014) (Sturdevant et al., 2015) (Heath et al., 2009) as the bulk of the replication occurs in structured lymphoid tissues (Folkvord et al., 2005)(Hufert et al., 1997)(Schacker, 2008). Compartmentalization creates smaller populations more susceptible to genetic drift. In these smaller, more stochastic populations, the fittest variant would not necessarily fix in the population. Instead, less fit variants would be able to establish locally when drift overpowers selection. In this scenario, mutation would play an important role in generation diversity. Mutation rates may vary over the HIV genome, due to differential rates of hyper-mutation by APOBEC (Kim et al., 2014)(Wood et al., 2009) and reverse transcriptase's lack of fidelity over particular stem loop structures (Cuevas et al., 2015) (Geller et al., 2015). Shannon entropy may be detecting differential diversity that is a signature of these uneven mutation rates. Shannon entropy may not simply be detecting signatures of functional and structural plasticity alone.

2.3.2 Reversions as a proxy for fitness cost: considerations

Alternatively, our reversion rates could be poor proxies of fitness. This might be due to the fact that samples were only taken post sero-conversion in the patients. A large window period measuring 20-30 days occurred between the time the patient first contracted HIV and had their blood sampled. Many highly conserved positions may have already reverted during this period. Therefore, a large subset of rapid reversions may be absent from our estimates. If this subset is large, we could possibly be grossly underestimating the average fitness costs at many positions. Secondly, we only observed consensus sequences out-replicating variants carrying typically only one residue type. The rate of reversion is likely residue dependent. However, even so it is concerning that on average, entropy does not predict reversion rate well.

2.3.3 Confounding factors to be explored in further analysis: immune pressure and epistasis

Two confounding factors must be taken into account when attempting to derive a fitness landscape from intra-patient longitudinal sequence data. First a residues fitness is highly dependent on the particular genetic background it is embedded in and second, immune pressure is heavily shaping the evolution of our population. The disappearance of viruses' bearing a particular residue may not be a sign that the residue is unfavorable for the virus to carry, instead it may indicate that the immune system more readily recognizes epitopes bearing that particular residue. In that case, even an intrinsically favorable residue may disappear from the population. White blood cells called T-cells play a central role in reducing viral loads during the acute portion of HIV infection (Borrow et al., 1994) (Ogg et al., 1998).Sometimes it is unclear whether a variant is disappearing because it is unfit, or if it is being targeted by the immune system. Immune system clearance of a variant can often be observed in patient kinetic data, with variants peaking in frequency during the first portion of the acute infection and then being eradicated during the second portion (Novitsky et al., 2009) (Liu et al., 2012).However, even in the absence of immune pressure, a residue's fitness may be shifted or hijacked by the mutational status of surrounding residues. In fact, simultaneous and tandem mutations are often observed within viral populations due to shared structural and or functional constraints (Ferguson et al., 2013)(Brockman et al., 2007)(Schneidewind et al., 2007)(Dahirel et al., 2011). Because of this, the cost of a mutation cannot not be ascertained from simply observing how single residue mutants replicate. The mutational status of the residues our position is coupled may need to be taken into account as well. It could be that a residue mutation is normally neutral in isolation, but in the presence of a neighboring mutation it is rendered unfit. It should be noted we have accounted for the first confounding factor in this analysis but not the latter.

Acknowledgments

We are grateful to all members of the primary HIV-1 subtype C infection study in Botswana (Tshedimoso Study) (Novitsky et al., 2011). We would also like to acknowledge the Theoretical Biology and Biophysics Division at Los Alamos National Laboratory for the HIV compendium and alignments made available by their group https://www.hiv.lanl.gov. The HIV Compendia are funded by the Division of AIDS, National Institute of Allergy and Infectious Diseases, through an interagency agreement with the U.S. Department of Energy. This work was supported in part by an NSF IGERT: Scalable Computing and Leading Edge Innovative Technologies (SCALE-IT) for Biology NSF Award Number 0801540.

2.4 Supporting Information

reversion

differential equations

$$\dot{W} = rW - \mu_w rW + \mu_m r(1-c)M \tag{2.16}$$

$$\dot{M} = r(1-c)M + \mu_w rW - \mu_m r(1-c)M \tag{2.17}$$

closed form solution

$$f_w(t) = \frac{f_0}{(1-f_0)e^{-crt} + f_0} \tag{2.18}$$

reversion with effector response

differential equations

$$\dot{W} = rW - \kappa EW - \mu_w rW + \mu_m r(1-c)M \tag{2.19}$$

$$\dot{M} = r(1-c)M + \mu_w rW - \mu_m r(1-c)M \tag{2.20}$$

$$\dot{E} = \alpha E \tag{2.21}$$

closed form solution

$$f_w(t) = \frac{f_0 e^{\frac{\lambda}{\alpha}}}{(1-f_0)e^{\frac{\lambda e^{\alpha t}}{\alpha} - crt} + f_0 e^{\frac{\lambda}{\alpha}}} \lambda = \kappa E_0 \tag{2.22}$$

growth constant $r = \ln(2)/T = 1$ where T is the doubling time of the virus. The assumption $\mu_w = \mu_m = 0$ can be make for large population sizes.

2.4.1 Immune Equation Derivation

If we assume the mutation rate has a neglible impact on our estimate of c due to large populations sizes, we can ignoring the mutation in and out of the consensus/wild W and non-consensus/mutant populations M, then we can write

Table 2.2: State Variables and Parameters The following parameters and state variables are shared between the two ODE Models

parameters	
f_w	frequency of wild variant
f_0	initial frequency of wild variant
μ_w	mutation rate of wild into mutant population
μ_m	mutation rate of mutant into wild population
c	replicative cost of mutation
r	growth constant of wild variant
κ	killing rate of effector cells
α	expansion rate of effector cells
state variables	
M	rna copies of mutant variant per ml of blood
W	rna copies of wild variant per ml blood
E	effector response of immune system

$$\dot{W} = rW - \kappa EW \tag{2.23}$$

$$\dot{M} = r(1-c)M \ \dot{E} = \alpha E \tag{2.24}$$

If we solve the effector differential equation assuming that at $E(0) = E_0$ we obtain the following solution to the below equation.

$$\dot{E} = \alpha E \tag{2.25}$$

which solves as:

$$E(t) = E_0 e^{\alpha t}. \tag{2.26}$$

We can than write the change in W and M as:

$$\dot{W} = rW - \kappa E_0 e^{\alpha t} W \tag{2.27}$$

$$\dot{M} = r(1-c)M \tag{2.28}$$

We wish to obtain a closed-form solution that describes the frequency of the variant:

$$f_w = \frac{W}{M+W} \tag{2.29}$$

We can rewrite f_w as:

$$f_w = \frac{\frac{W}{M}}{1 + \frac{W}{M}} \tag{2.30}$$

We can solve easily for this ratio of W to M. We will call this $z(t) = \frac{W(t)}{M(t)}$. We know that the derivative of z is:

$$z'(t) = \Big(\frac{W}{M}\Big)\frac{d}{dt} = \frac{M\dot{W} - W\dot{M}}{M^2} \tag{2.31}$$

substituting in the respective differential equations we obtain

$$\Big(\frac{W}{M}\Big)\frac{d}{dt} = \frac{M\Big(rW - \kappa E_0 e^{\alpha t} W\Big)}{M^2} - \frac{W\Big(r(1-c)M\Big)}{M^2} \tag{2.32}$$

Cancel out terms and group $\frac{W}{M}$ ratios

$$z'(t) = \Big(r - \kappa E_0 e\{\alpha t\} - r(1-c)\Big)z(t) \tag{2.33}$$

which simplifies to

$$z'(t) = \Big(- \kappa E_0 e\{\alpha t\} + rc\Big)z(t) \tag{2.34}$$

We can then solve for the ratio z in this separable equation:

this gives us a solution of:

$$z(t) = z_0 \cdot e\{\Big(\frac{-\kappa E_0 e^{\alpha t}}{\alpha} + \frac{\kappa E_0}{\alpha} + rct\Big)\} \tag{2.35}$$

The solution to f_w is then:

$$f_w(t) = \frac{z(t)}{1 + z(t)} \tag{2.36}$$

Which when substituting z,

$$f_w(t) = \frac{z_0 \cdot e^{\frac{-\kappa E_0 e^{\alpha t}}{\alpha} + \frac{\kappa E_0}{\alpha} + rct}}{1 + z_0 \cdot e^{\frac{-\kappa E_0 e^{\alpha t}}{\alpha} + \frac{\kappa E_0}{\alpha} + rct}} \tag{2.37}$$

Writing z_0 in terms of f_0 we see that,

$$f_w(t) = \frac{e^{\frac{\kappa E_0}{\alpha}}}{\frac{1-f_0}{f_0} \cdot e^{\frac{\kappa E_0 e^{\alpha t}}{\alpha} - rct} + e^{\frac{\kappa E_0}{\alpha}}} \tag{2.38}$$

If we group the clearance rate κ and the initial effector population E_0 we are then only fitting four parameters ($\kappa E_0 = \lambda$).

$$f_w(t) = \frac{f_0 e^{\frac{\lambda}{\alpha}}}{(1 - f_0) e^{\frac{\lambda e^{\alpha t}}{\alpha} - crt} + f_0 e^{\frac{\lambda}{\alpha}}} \tag{2.39}$$

$$\lambda = \kappa E_0 \tag{2.40}$$

Chapter 3

Fitness Map constructed using a physico-chemical model of residue substitution

Abstract

Quantifying the variation in the strength of purifying selection across a protein sequence is of fundamental interest in both structural and evolutionary biology. Here we present a simple, quantitative model grounded in the field of population genetics that allows one to estimate the optimal amino acid sequence of a protein and the sensitivity of the protein's functionality to deviation from this optimal sequence in physicochemial space. Conceptually, our model can be viewed as constrained version of a model describing residue conservation, where, in our model, the link between protein sequence (genotype), protein function (phenotype), and fitness are explicitly, rather than implicitly, modelled. We use maximum likelihood to parameterize our model using over a 1000 different sequences of HIV subtype C's Gag poly-protein. We evaluate its performance by comparing our amino acid site specific sensitivity parameters to empirical *in vitro* and *in vivo* measures of HIV fitness. To better contextualize our results, we first show how frequently used, entropy metrics can be viewed as a generalization and fully saturated version of our model. Second, we fit the entropy model to the same sequence data and evaluate its ability to predict the same empirical fitness data. In terms of fitting the sequence data, AIC indicates that the entropy model substantially outperforms our model. This result is not surprising given the entropy model has as many parameters as categories and, by definition, the best model possible for any categorical data set and that we fit the models using more than 50 data points per parameter. In contrast, we find that our model's site sensitivity parameters do a better job predicting the empirical fitness data than the entropy model's site specific conservation terms. Thus, while the entropy model may fit the sequence data better, our model appears to better contextualize the information encoded within that data. This result is also not surprising given the fact that our model's site specific sensitivity parameter has a direct biological interpretation while the entropy model's conservation term is simply a measure of mean uncertainty of the state of a site. More importantly, unlike the entropy model, our model can be further refined and used to test more complex hypotheses about the link between genotype, phenotype, and fitness. For example, in our analysis we find evidence that different functional regions of the gag poly-protein have different sensitivities to deviation from the optimal amino acid's molecular volume.

3.1 Introduction

3.1.1 Fitness Landscapes and HIV Diversity

HIV exhibits a great deal of genetic plasticity (Lemey et al., 2006; Salemi, 2013; Cuevas et al., 2015). This genetic plasticity allows the virus to effectively evade a patient's immune response and has accordingly aggravated attempts to create an effective vaccine immunogen (Goulder and Watkins, 2004; Autran et al., 2008; Johnston and Fauci, 2008). While an immunogen might elicit a strong CTL response against an HIV epitope, the virus can often avoid this immunogen elicited recognition by mutating the targeted epitope. In a genetically plastic virus such as HIV, not every mutation incurs a serious fitness penalty. As a consequence, mutationally robust positions along the proteome tend to be the ones to escape immune recognition (Korber et al., 2001; Hinkley et al., 2011). However, there are vulnerable regions along the proteome that are expensive for the virus to mutate (Martinez-Picado et al., 2006; Rihn et al., 2013; Manocheewa et al., 2015). In order to identify these vulnerable regions, mutational landscapes for the viral proteome have been constructed (Deforche et al., 2008; Seifert et al., 2015; Kouyos et al., 2012; Hinkley et al., 2011; Shekhar et al., 2013; Ferguson et al., 2013; Mann et al., 2014; Lorenzo-Redondo et al., 2014; Moradigaravand et al., 2014; Barton et al., 2016). These mutational landscapes describe the sum or synergistic replicative cost exacted on the virus for any combination of residue level mutations (Michael R. Dietrich, 2012; Acevedo et al., 2014). They can be constructed using a variety of approaches, both indirectly by computational analysis of patient sequence data (Ferguson et al., 2013) and directly using *in vitro* methods such as growth competition assays (Manocheewa et al., 2015).

Predict escapes is bench-marked on a longitudinal data set detailing viral within-host dynamics. Using a cross-sectional MSA, we can generate a fitness landscape using a population genetics model derived from work by Gilchrist et al. (2009); Gilchrist (2007) and Shah and Gilchrist (2011). In this formulation, the frequency landscape of residues in the proteome informs the construction of the fitness landscape but does not directly underlay it as it does in entropy maximization frameworks. Instead, the functional impact of the residue level mutations are taken into account. To estimate functional impacts, a physico-chemical distance measurement is employed to gauge how different a mutant residue is from the estimated optimal residue. Physico-chemical attributes considered in the distance measurement includes properties such as polarity, charge, and size. These properties have been shown to be predictive of residue substitution frequencies in many species Grantham (1974). Taking this distance measurement, we combine it with derivations from Sella and Hirsh (2005) which elegantly link the relationship between frequency and fitness in a population genetics framework. This formulation allows us to 1) describe the HIV fitness landscape with fewer parameters than classical Shannon entropy based calculations and 2) avoid using frequency as the singular signature of fitness.

3.2 Methods

3.2.1 Shannon Entropy

$$w_{ij} \propto \frac{x_{ij}}{N} \tag{3.1}$$

$$p_{ij} = \frac{w_{ij}}{\sum\limits_{j=1}^{20} w_{ij}} \tag{3.2}$$

$$E_i(X) = -\sum_{j=1}^{20} p_{ij} \ln p_{ij} \tag{3.3}$$

The term x_{ij} is the number of residues j observed at position i in the cross-sectional sample of sequences. The fitness w_{ij} of any particular amino acid residue j at position i is proportional to the number of residues j observed at that position (x_{ij}) divided by the total number of residues observed N. We can then write the probability (p_{ij})of observing each of the residue's given the residues proportional relative fitness compared to the total relative fitness of the other residues. The entropy of the position defined by those probabilities E_i is defined by equation 3.3.

3.2.2 Estimating Physico-chemical Sensitivities

In the model, the fitness w_{ij} of an amino acid j at position i is proportional to an exponential decay function (eq. 3.4). This function, decays as the Physico-chemical distance D_{ij} increases between the amino acid a_j and the consensus amino acid a_i for that position (eq. 3.5). The sensitivity parameter G' describing how sensitive the virus is to deviations from the consensus residue at this position.

$$w_{ij} \propto \exp[-G'_i \cdot D(\vec{\theta}, a_i, a_j)] \tag{3.4}$$

Physico-chemical deviation between residues i and j are measured in terms of differences in composition c_i, polarity p_i, and molecular volume v_i, using the weightings θ_c,θ_p, and θ_v respectively. It should be noted that these three properties are not necessarily independent of each other. However, for the sake of simplicity, the properties of composition, polarity and molecular volume are treated as independent and therefore orthogonal to each other in the distance calculation for D (eq. 3.5).

$$D(\vec{\theta}, a_i, a_j) = [\theta_\alpha(c_i - c_j)^2 + \theta_\beta(p_i - p_j)^2 + \theta_\gamma(v_i - v_j)^2]^{1/2} \tag{3.5}$$

These three properties are used because residues that share one of these three properties are more likely to be interchanged with each other according to residue substitution frequencies (RSF). Values for these properties were taken from Grantham (Grantham, 1974) and the weighting of each of these properties was estimated specifically for HIV using a MLE on sequence data.

We can calculate the probability of observing an amino acid by partitioning the relative frequency of the amino acid by the sum total of all the relative amino acid frequencies for the position. The relative frequency of an amino acid at a position can be expressed in terms of fitness and population size. The value w_{ij} in (eq. 3.6) describes the fitness of amino acid i at position j relative to other amino acids. However it is not sufficient to describe the probability of drawing an amino acid in terms of relative fitness alone. Due to drift, we would expect the frequency of a less fit amino acid to be higher in smaller populations and lower in larger ones. To account for this, the value w_{ij} is modulated by the effective population size N_e to obtain a relative amino acid frequency for the position. This model is different than the Ising model in that it is derived from a population genetics framework, and incorporates more biological information in order to calculate the decay term with the exponential.

$$p_{ij} = \frac{(w_{ij})^{Ne}}{\sum\limits_{j=1}^{20} (w_{ij})^{Ne}} = \frac{\exp[-N_e \cdot G'_i \cdot D(\vec{\theta}, a_i, a_j)]}{\sum\limits_{j=1}^{20} \exp[-N_e \cdot G'_i \cdot D(\vec{\theta}, a_i, a_j)]} \tag{3.6}$$

We can regard the resulting formulation (eq. 3.6) as a type of Boltzmann distribution with fitness corresponding to energy, and population size corresponding to heat. Sella and Hirsh demonstrated in their 2005 paper Sella and Hirsh (2005) that the Boltzmann distribution, used to describe state distributions in a thermodynamic systems, had analogous application to genotype distributions in evolutionary systems. However, our data does not allow us to tease apart population (N_e) and sensitivity (G') effects. We therefore group the two terms together as G'', scaling mutational sensitivity by effective population size (eq. 3.7).

$$p_{ij} = \frac{\exp[-G''_i \cdot D(\vec{\theta}, a_i, a_j)]}{\sum\limits_{j=1}^{20} \exp[-G''_i \cdot D(\vec{\theta}, a_i, a_j)]} \tag{3.7}$$

The likelihood function

$$\mathcal{L}(G''_i, \vec{\theta} \mid X) = \frac{\Gamma(\sum_j x_{ij} + 1)}{\prod_j \Gamma(x_{ij} + 1)} \prod_{j=1}^{20} p_{ij}^{x_{ij}} \tag{3.8}$$

Table 3.1: Parameters and Variables for Physico-Chemical Model The following parameters are shared between the models used to approximate strong stabilizing selective pressure along the protein.

w_{ij}	relative fitness of amino acid j at position i.
x_{ij}	number of sequences with amino acid j at i
N_e	effective population size
G'_i	sensitivity of the position i to deviation
G''_i	G'_i scaled by effective population size.
$D(a_i, a_j)$	Physico-chemical distance between two residues
p_{ij}	probability of observing amino acid j at position i
X	the Multiple Sequence Alignments
θ_α	composition weighting
θ_β	polarity weighting
θ_γ	molecular volume weighting

3.2.3 Model Parameterization

Because G'' is always multiplied by our distance function d, there is an inherent lack of identifiability in our model. To solve this problem, $\vec{\theta}$ was constrained so that the sum of its values equaled 1. In order to identify a reasonable starting set of sensitivity values G'' for the sites, we first optimized our physio-chemical model by fixing our physicochemical weights $\vec{\theta}$ to the values identified by **?**. We then parameterized our physicochemical model using a two stage shotgun hill climbing optimization implemented using SCIPY packages **?**. Briefly, for a given set of $\vec{\theta}$ values, we optimized G'' and the optimal amino acid for each site. We did so by finding the optimal G'' value for each amino acid HXB2 coordinate using a sequential least squares programming iterative method SLSQP. We then chose the combination of the optimal amino acid and G'' with the largest log likelihood. We then used a constrained optimization by linear approximation COBYLA algorithm to optimize over $\vec{\theta}$ space, re-optimizing G'' and the optimal amino acid at each step as described above.

The optimization was first initialized at $>$50 random weights in the physicochemical weight space $\vec{\theta}$. The weight space was explored for a constrained number of optimization steps to assess the most likely combination of weights around the initialized points. For each step in this exploration, the G'' sensitivities were re-optimized for that particular set of weights. After this exploration routine, the shotgun hill climbing optimization was reinitialized for the top three sets of physicochemical weights obtaining the highest likelihoods. The optimization algorithm was reinitialized from these regions of physico-chemical weight space and was allowed to run until convergence. The most likely parameter weight combination from this optimization step was then selected. The optimization for the G'' values was initialized as a grid search using a vector containing a distribution of likely G'' values. This distribution of likely G'' values was obtained from an optimization in which the physicochemical weights were regarded as similar to those estimated from (Grantham, 1974) paper examining general residue substitution frequencies across species. We regarded the maximum likelihood set of parameter weight combinations from the convergence of these optimization to be our global optimum. In order to test whether the same $\vec{\theta}$ values were applicable across all sites, we compared our model fit with a single set of $\vec{\theta}$ values to one where $\vec{\theta}$ was allowed to vary between the functional regions p24, p17, p7, and p6.

3.2.4 Cross-sectional Sequences

We use 1000 curated sequences in the Los Alamos database for subtype C http://www.hiv.lanl.gov/. These sequences were filtered web alignments that provide a good example of the subtypes breadth. Every sequence belongs to a unique patient and sequences that resemble each other too closely had been removed. Additionally questionable sequences such as those that appear to be hypermutants and synthetics have also been removed. The curated sequences were clean, containing little ambiguous coding, few long insertions and lacked a preponderance of frame shifts.

Sequences in this curated alignment were aligned using both automation (HMMER) and manual editing. Sequences were processed to obtain amino acid counts for each HXB2 coordinate. These counts were augmented by the full set of natural amino acids to obtain a lower bound estimate on hyper-conserved positions.

3.2.5 Assessing Concordance of Physico-chemical Sensitivity with Shannon Entropy

We sought to assess how well shannon entropy correlated with physico-chemical sensitivity in different functional regions of the protein (p24, p17, p6 and p7). We then sought to see if correlation was influenced by the character of the functional regions secondary structure.The map of secondary structure to HXB2 coordinates was conducted using the HIV mutation browser (**?**). Two non-parametric rank correlation coefficients (Kendall's τ and Spearman's ρ) were used assess the monotonicity of the relationship between shannon entropy and physico-chemical sensitivity. We employed Spearman's correlation statistic due to its familiarity and Kendall's correlation statistic due to its superior robustness, interpretable coefficient, and sound confidence intervals (Kendall and Gibbons, 1990; Croux and Dehon, 2010).

3.2.6 Characterizing Distribution of Sensitivities

Three candidate density models gamma, lognormal, and inverse-gamma were fit by maximum likelihood estimation to the distributions of sensitivities (G''). This was done in order to determine which density distribution best characterized the mutational sensitivity along the protein and along the individual functional regions. We then conducted an AIC test to determine if the distributions were distinct for the functional regions (H_A) or if selection along the protein was homogenous (H_0). The alternative regional model required six additional parameters. The relative likelihood or weight of evidence (w_i) for the next best fitting model was then calculated using the below equation where i denotes the model with the larger AIC (bur, 2002).

$$w_i = \exp\left[\frac{AIC_{min} - AIC_i}{2}\right] \tag{3.9}$$

3.2.7 Predicting Viral Behaviors

Correlation with in vivo escape times

Entropy scores can help predict how long it will take the virus to escape a CD8 T-cell response. (Liu et al., 2012). It has been shown that high entropy epitopes can more easily escape immune targeting while low entropy epitopes struggle to evade immune detection or escape slowly (Ferrari et al., 2011). In this analysis, we test whether our physico-chemical sensitivity (G'') or shannon entropy (S) better predicts escape times. The escape times used in this analysis come from a 2012 paper by Liu et al. (2012) where viral escapes at reactive epitopes sites were characterized in 17 HIV-1 subtype B infected patients over 3 years using serial SGA sequencing. In this analysis, the predicted variabe escape time (t_{50}) is defined as the number of days between detection of the T-cell response and the time viral variants bearing that respective reactive epitope fell below 50%.

Correlation with in vitro viral spreading fitness

Entropy scores can be used to predict how a mutation will impact the replicative capacity of HIV In this analysis, we tested whether our physico-chemical sensitivity (G'') or shannon entropy (S) better predicted replicative fitness costs exacted on mutants. Rihn et al. (2013) assessed the replicative fitness of HIV virions bearing various capsid (CA)mutations via spreading replication assays on human T-cell lines (MT4) and PBMC. The CA mutants in this study were generated by creating a mutagenized CA library using a low fidelity PCR approach and then inserting the mutated CA sequences in replication competent proviral clones. Fitness was reported as % of the wild-type replication as recorded by the number of GFP fluorescing cells.

3.3 Results and Discussion

3.3.1 Physico-chemical selective forces vary along the poly-protein

It was unclear if the the physicochemical selective forces shaping residue evolution varied along the Gag poly-protein. Two candidate models were compared to inspect the variation. In the alternative model H_A the physicochemical selective forces as described by the weighting vector $\vec{\theta}$ were free to vary by region. In the null model H_0, it was assumed that selective forces $\vec{\theta}$ were uniform over the protein. Surprisingly, even slight adjustments to the physicochemical weights on a per-region basis (Table 3.10) significantly improved the model's ability to describe the observed residue frequencies in our MSA by several loglikelihood units (Table 3.2)

Table 3.2: Model Selection Likelihood Ratio Test assessing single (H_0) vs regional (H_A) physico-chemical weighting

$Log(\mathcal{L})\ H_0$	$Log(\mathcal{L})\ H_A$	LRT test statistic	df	p-value
-69040	-63550	10980	6	<2.23e-308

This variation likely stems from differences in secondary structure composition among the regions. It has been shown that amino acids can be clustered by alpha helices/turn and beta sheet propensity (kawashima,2000) as each structure possesses inherently different physico-chemical constraints. These particular properties (molecular volume, polarity and composition) are just three among a host of side chain properties that may be similarly predictive of residue interchangeability. This set of properties was initially chosen because they were good correlates of residue interchangeability in organisms other than HIV (Grantham, 1974). In the previous paper these estimates were derived from residue substitution frequencies. Finally, the inter-property correlations between the side-chain traits imply that these weighting estimates are similarly not entirely independent of each other.

Given that the traits of composition, polarity, and molecular volume may not be the principle selective forces determining residue interchangeability and fixation, further work should pursue identifying other traits that appreciably improve the model's ability to describe residue frequency in a sampled viral poplulation. Contending traits include continuous properties like hydrophobicity or acidity and categorical traits such as the aliphatic or aromatic side chain construction.

3.3.2 Distributions of Physico-Chemical Sensitivities

Lognormal model best describes distribution of sensitivities

Out of three candidate density models (gamma, lognormal, inverse-gamma), the lognormal model optimally described the distribution of sensitivites over the poly-protein (Table 3.3).The exception was p7, in which the gamma fit was slightly better. The generative process underlying this distribution is one in which many positive random independent variables act proportionally on each other. Many biological phenomena are well described by this type of process. The parameters of this model are readily interpretable as the logarithm of a lognormal distribution X is simply a normal distribution. This normal distribution can be described by a location value μ where values around μ are shifted by a standard normal random variable Z scaled by a shape parameter σ (eq. 3.10).

$$X = e^{\mu+\sigma Z} \tag{3.10}$$

Character of sensitivity distributions differ between functional regions

Under this new model, it was unclear if the fitness proxy's (G'') distribution would retain a distinct character from one region to the next or if the fitness proxy's distribution would appear

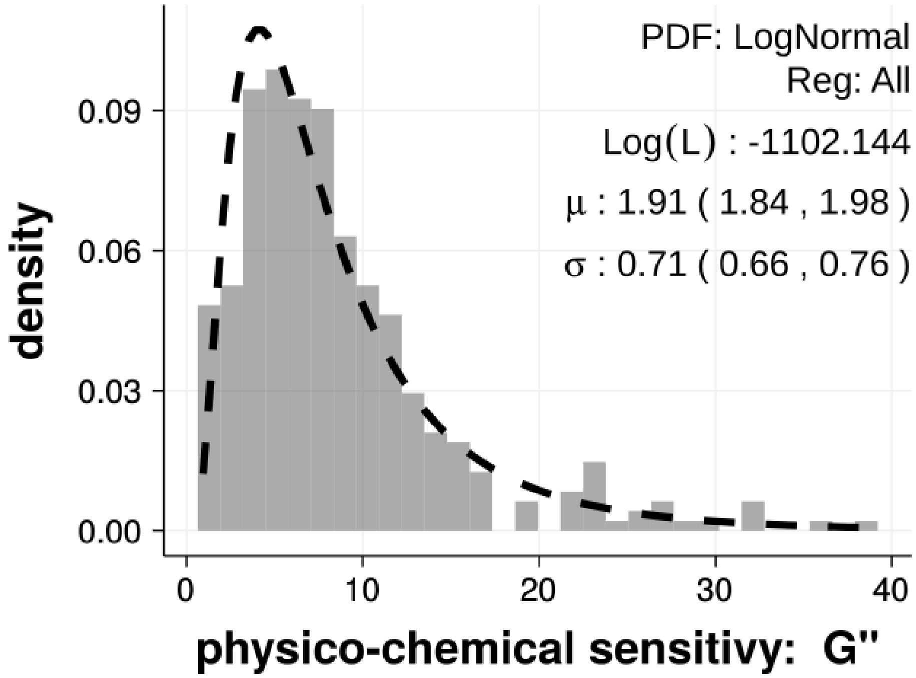

Figure 3.1: Distribution of physico-chemical sensitivities for Gag Polyprotein The distributions of G'' sensitivities are described with a Lognormal model. Regional location μ and scale σ parameters identified via MLE. Distribution excludes spacer regions and includes regions p17,p24,p7 and p6 (n= 370). Hyper-conserved outlier positions (conservation value (1/E) >100) were excluded

Table 3.3: Likelihood of PDF Models Shows likelihood of Gamma, Lognormal and Inverse Gamma continuous probability distributions for the G'' sensitivity values for residues along the Gag poly-protein.

Region	$Log(\mathcal{L})$ Gamma	$Log(\mathcal{L})$ Inverse Gamma	$Log(\mathcal{L})$ Lognormal
All	-1104	-1132	-1102
p17	-340.2	-345.4	-337.8
p24	-504.9	-510.9	-502.5
p6	-118.8	-117.7	-116.5
p7	-115.9	-123.6	-118.4

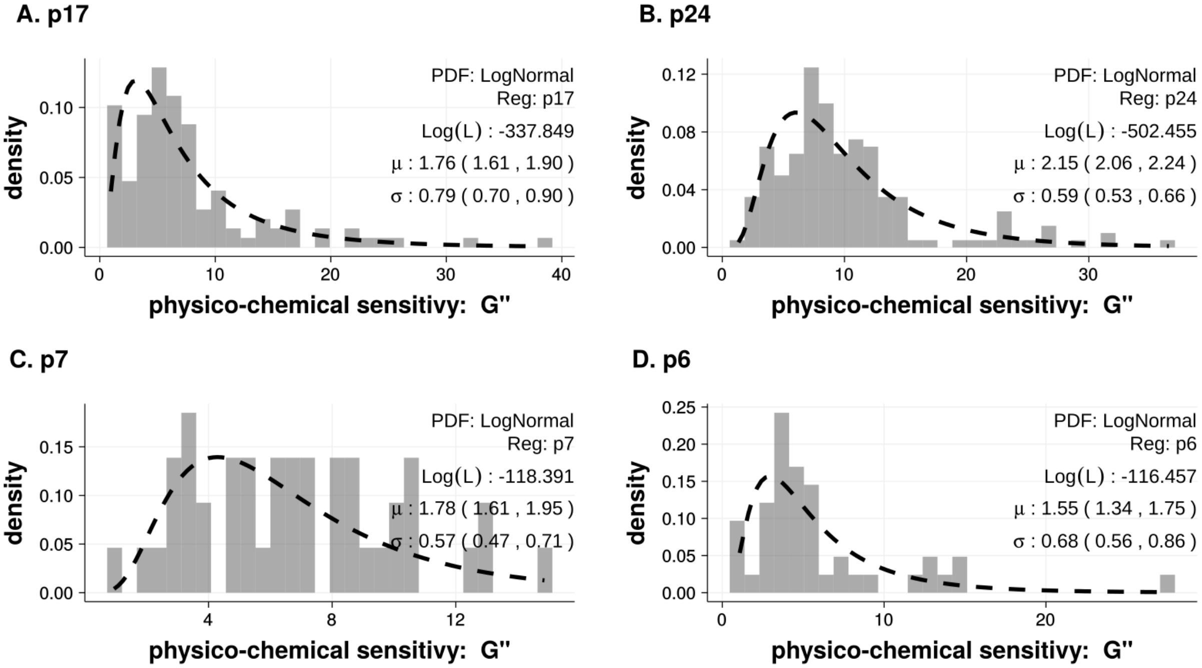

Figure 3.2: Distribution of physico-chemical sensitivities The distributions of G'' sensitivities are described with a Lognormal model. Regional location μ and scale σ parameters identified via MLE. **A.p17** Lognormal PDF describing distribution of physico-chemical sensitivities for the Matrix. **B.p24** Lognormal PDF describing distribution of physico-chemical sensitivities for the Capsid. **C.p7**) Lognormal PDF describing distribution of physico-chemical sensitivities for the Nucleo-capsid. **D.p6**) Lognormal PDF describing the distribution of physico-chemical sensitivities for the Nucleoprotein.

homogeneous over the poly-protein. To address this question, a lognormal PDF was fit to the distribution of sensitivities in p6,p7,p17 and p24 to capture the distinctive character of the regional distributions. This fitting provided the location μ and shape σ parameters describing the lognormal distribution for each region along with 95% confidence intervals calculated from log-likelihood profiles of the the MLE . These results show that the lognormal distribution of physico-chemical sensitivities is distinct for the functional regions p17 and p24 given that the descriptive location and shape parameters of the confidence intervals do not overlap (Fig. 3.3).

Table 3.4: LogNormal Fits of Physico-Chemical Sensitivities The distribution of physico-chemical sensitivities were described by a lognormal distribution for functional regions p17,p24,p7 p6 and all the regions collectively. The MLE for the lognormal shape parameters (μ,σ) are displayed for each region. The estimates are displayed with 95% confidence intervals calculated from the parameter's likelihood profile.

Region	Log Likelihood	μ	σ
All	-1102.14	1.909 (1.837,1.981)	0.705 (0.657,0.759)
p17	-337.85	1.756 (1.610,1.901)	0.789 (0.697,0.903)
p24	-502.46	2.150 (2.059,2.241)	0.592 (0.534,0.662)
p7	-118.39	1.779 (1.609,1.948)	0.567 (0.468,0.708)
p6	-116.46	1.547 (1.343,1.752)	0.685 (0.565,0.855)

To establish whether the distribution of physico-chemical values varied regionally, we also evaluated two candidate models describing the distribution of the sensitivities. One model described the distribution of sensitives on the poly-protein collectively with a single Lognormal PDF and the other described the sensitivities using a set of regional Lognormal distributions (Table. 3.11). Each model's likelihood was computed on the same set of sensitivities and the most appropriate model was selected by comparing the corresponding AICs (Table 3.5) . From these results we can infer that we have sufficient support for preferring the more complex regional model over the simple collective model which has a relative likelihood of 7.65×10^{-10}.

Both the lognormal parameter evaluation and the model selection procedure above reveal that the poly-protein's functional regions possess distinct distributions of physicochemical sensitivities.

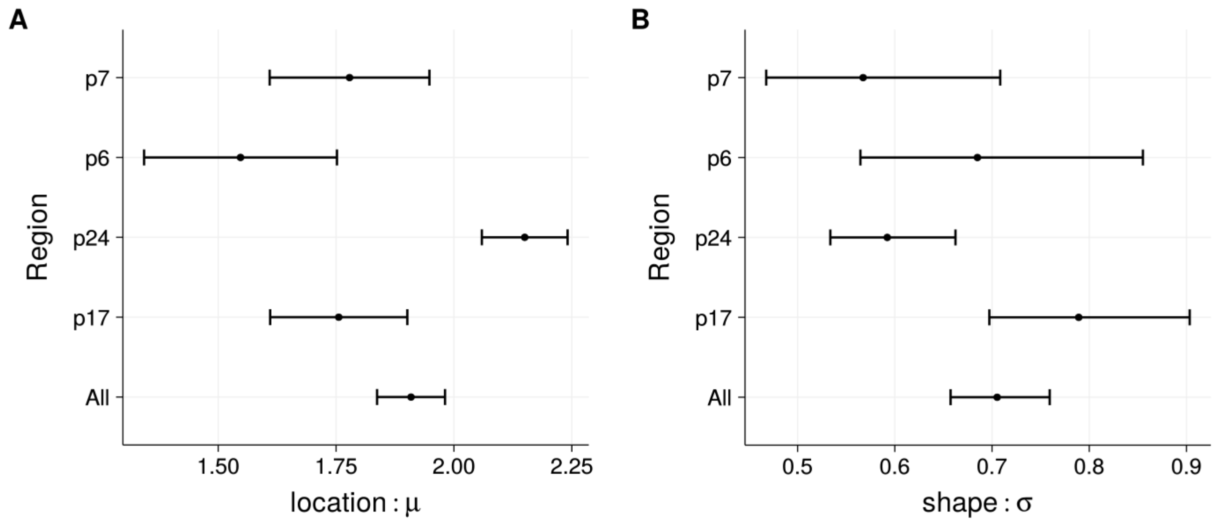

Figure 3.3: MLE of Lognormal parameters for each region Panels display Lognormal parameter fits for each region and all regions collectively. **A.** The location parameter for the capsid's (p24) distribution is statically higher compared to the other regions and the nucleocapsid's (p7) distribution is statistically lower than the poly-protein's (All) distribution. **B.** Shows location parameter σ for each region with 95% confidence intervals estimated by likelihood profiling. The capsid (p24) and matrix (p17) distributions have a shape parameters distinct from each-other

This finding suggests that the landscape of fitness costs is not uniform over the poly-protein, and instead may display a unique character from functional region to functional region.

Table 3.5: Model Selection for Regional vs Poly-Protein Model of Sensitivity Distributions The distribution of physico-chemical sensitivites are described via a single lognormal probability distribution function (H0) or via a family of lognormal distributions (HA) tailored to the proteins functional regions p17, p24, p7 and p6.

Model	No. Parameters	$Log(\mathcal{L})$	AIC	Δ AIC	Relative Likelihood
poly-protein	2	-1102	2208	41.98	7.65e-10
regional	8	-1075	2166	0	—

3.3.3 Assessing Concordance of Physico-chemical Sensitivity with Shannon Entropy

The estimated Physico-chemical sensitivity of a position correlated well with it's conservation overall (Fig 3.4), although the correlation varied by functional region (Fig 3.5). In particular, the nucleoproteins and matrix regions were more strongly correlated than the capsid and nucleocapsid (Table 3.7). This variation by regions is likely due to the secondary structure (strand,helix, or turns) that predominates in these regions. Shannon entropy and physico-chemical sensitives were not as strongly correlated in functional regions lacking secondary structure, with the exception of p6 which has no strands,helices or turns. This is likely because the regions have different percentages of secondary structure. This would make it difficult for our model to settle on a proper set of weights as there are probably different selective weight for each type of secondary structure (Table 3.6).

Table 3.6: Primary and Secondary Structure Correlation between methods (Kendall Tau) with primary and secondary structure. Secondary structure broken down by turn, helix and strand

Functional Region	Kendall tau	Secondary Structure	Primary	Turn	Strand	Helix
p7	0.3443	0.29	0.71	0.19	0.1	0
p24	0.4561	0.68	0.32	0.092	0.021	0.57
p17	0.6249	0.75	0.25	0.069	0.12	0.56
p6	0.7909	0	1	0	0	0

The reason shannon entropy and our sensitivity metric concord so strongly might be due to the lack of secondary structure in this functional regions (Fig. 3.6).

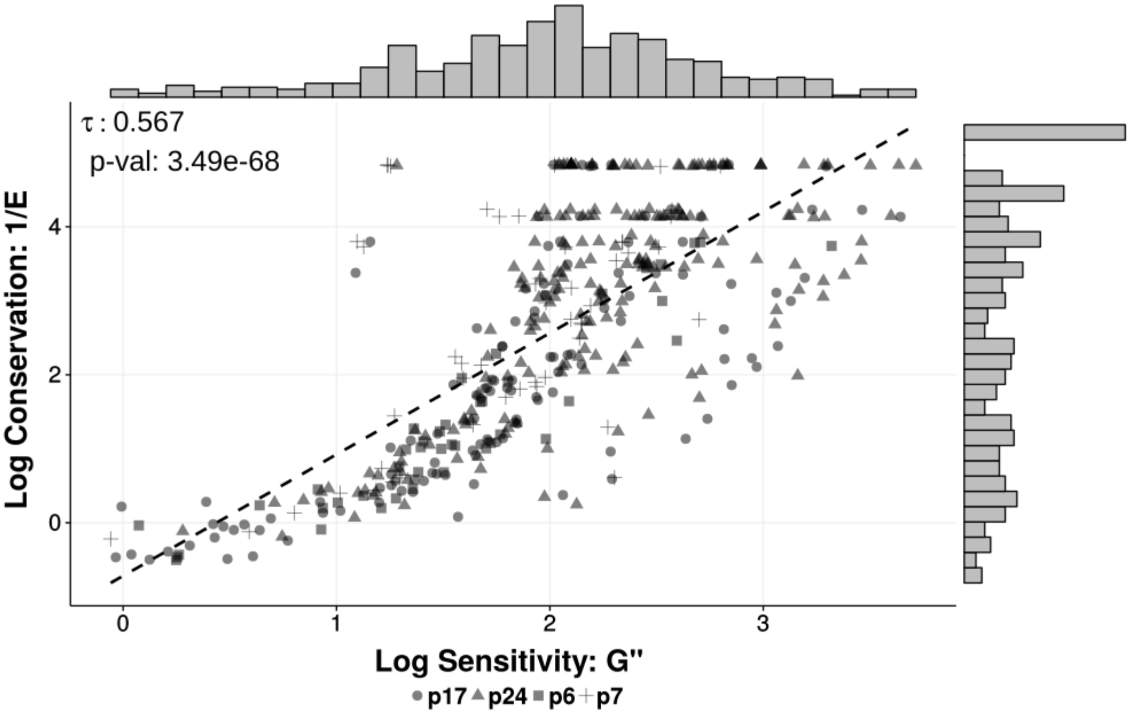

Figure 3.4: Rank correlation of each position's estimated physico-chemical sensitivity G'' with it's conservation ($1/E$). Positions total 520 in the Gag poly-protein excluding spacer regions. Estimates of sensitivity G'' and conservation $1/E$ estimated and derived from 1000 sample MSA of the Gag poly-protein for HIV-1 subtype C. Sensitivity and conservation concord with each other with a significant kendall τ of 0.567.

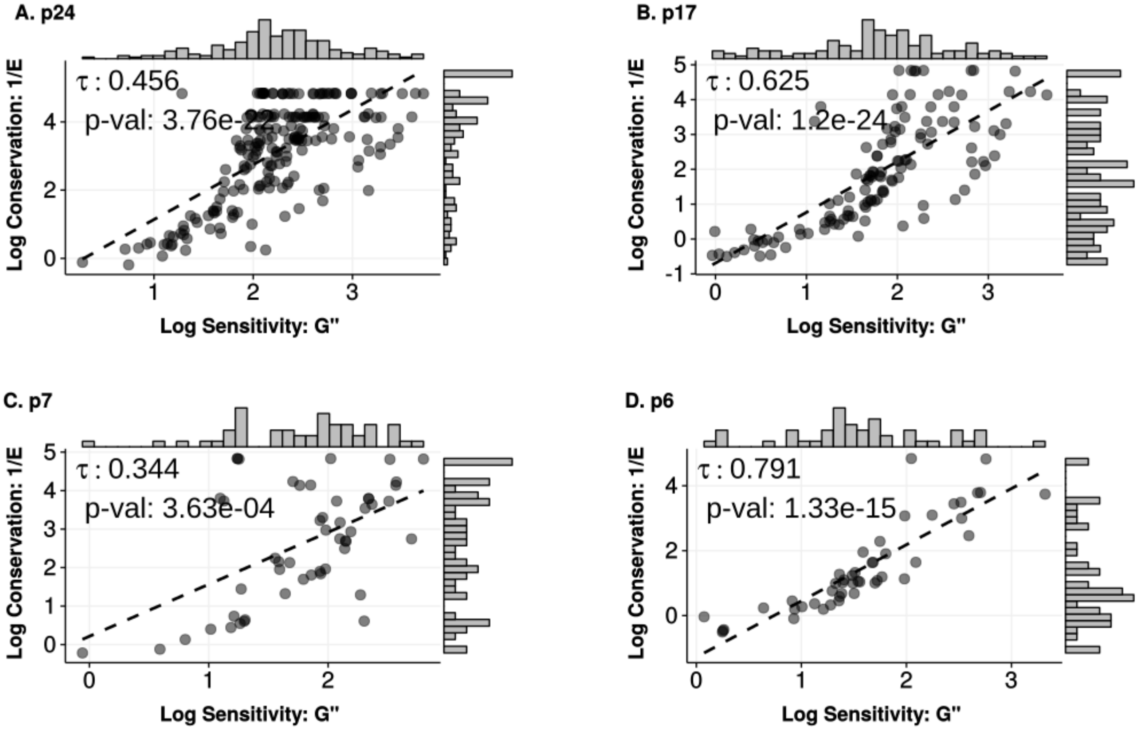

Figure 3.5: Rank correlation of sensitivity and conservation in the four functional regions in the Gag poly-protein A.p24) Concordance of sensitivity and conservation in the viral capsid $tau = 0.456$ **B.p17**) Concordance of sensitivity and conservation in the viral matrix $tau = 0.625$ **C.p7**) Weak concordance of sensitivity and conservation in the viral nucleo-capsid $tau = 0.344$ **D.p6**) Strong concordance of sensitivity and conservation in the viral nucleo-protein $tau = 0.791$. Estimates of sensitivity G'' and conservation $1/E$ estimated and derived from a 1000 sample MSA of the Gag poly-protein for HIV-1 subtype C.

Table 3.7: Correlation Statistics between Sensitivity and Conservation Table displaying correlation statistics between sensitivity (G') and conservation ($1/S$) for the poly-protein and each functional region

region	kendall tau	p-value	tau 95% CI
Gag	0.567	3.492e-68	(0.510 - 0.621)
p24	0.456	3.758e-22	(0.362 - 0.545)
p17	0.625	1.203e-24	(0.534 - 0.709)
p7	0.344	0.000363	(0.100 - 0.570)
p6	0.791	1.332e-15	(0.709 - 0.860)

region	spearman rho	p-value	rho 95% CI
Gag	0.7295	8.598e-72	(0.666 - 0.786)
p24	0.6101	3.446e-22	(0.493 - 0.710)
p17	0.7907	1.474e-27	(0.683 - 0.870)
p7	0.4192	0.002387	(0.107 - 0.693)
p6	0.9355	<2.23e-308	(0.866 - 0.963)

3.3.4 Predictive power of physico-chemical sensitivity on fitness effects

physico-chemical sensitivity metric vs shannon entropy predicting in vivo escape data

We used two nonparametric measures of rank correlation to assess how well an epitope's entropy and physico-chemical sensitivity correlated with its escape time from an immune response 3.6. Spearman's ρ and kendall's τ were positive for both correlations 3.8, but only the physico-chemical correlation had significant ρ and τ with p values of 0.042 and 0.046 respectively. We can interpret the significant τ of 0.230 as the percentage of of epitope pairs that have escape times trending in a positive direction with physico-chemical-sensitivity (65%). These results suggest that Physico-chemical sensitivity of an epitope is a better proxy for escape time than an epitope's entropy.

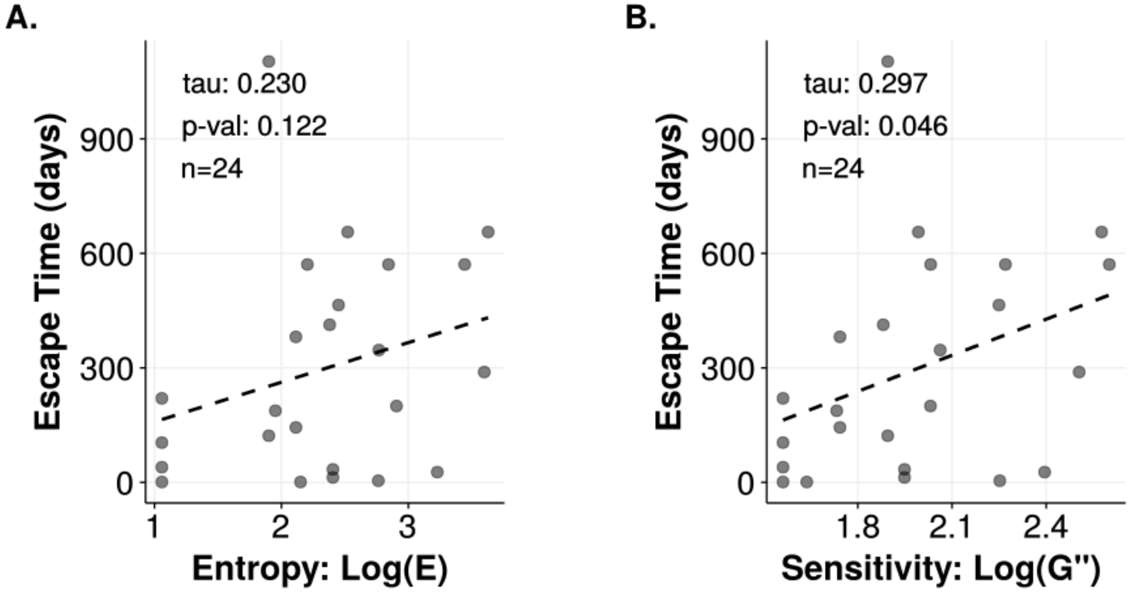

Figure 3.6: Correlation of entropy and sensitivity with the escape time of 24 epitopes in the Gag poly-protein A) Correlation of the escape time of an epitope in days with the epitope's entropy B) Correlation of the escape time of an epitope in days with the epitope's physico-chemical sensitivity.

Table 3.8: Correlation with Escape Time Table displaying correlation statistics between epitope sensitivity (G'') or entropy (S) and escape time

kendall correlation	kendall tau	p-value	tau 95% CI
Epitope Entropy vs. Escape Time	0.230	0.122	(-0.074 - 0.517)
Epitope Sensitivity vs Escape Time	0.297	0.046	(0.008 - 0.560)

spearman-rank correlation	spearman rho	p-value	rho 95% CI
Epitope Entropy vs. Escape Time	0.310	0.140	(-0.106 - 0.657)
Epitope Sensitivity vs Escape Time	0.418	0.042	(0.004 - 0.720)

physico-chemical sensitivity metric vs shannon entropy predicting in vitro viral spreading fitness

The replicative fitness of viruses bearing mutated capsid residues was assessed by Rihn et al. (2013) via spreading replication assays on human T-cell lines (MT4) and PBMC. (see methods **??**).In the below analysis, non-parmetric rank correlations were used to assess how well each residue position's entropy and physico-chemical sensitivity correlated with its assayed spreading fitness (Fig. 3.7). There was a significant negative correlation between both entropy vs spreading fitness (τ, p=0.038 & ρ, p= 0.0296) and sensitivity vs spreading fitness (τ,p=0.0021 ρ, p=0.0007) for both rank correlations. However, the physico-chemical sensitivity of the position more strongly correlated with the assayed spreading fitness with correlation coefficients of $\rho = -0.379$ and $\tau = 0.256$ for entropy but $\rho =$ -0.558 and $\tau =$ -0.381 for sensitivity (Table 3.9). These results suggest that Physico-chemical sensitivity of a residue position is a more robust proxy for assayed spreading fitness than positional entropy.

Table 3.9: Correlation between conservation and sensitivity Table displaying correlation statistics between epitope sensitivity (G') or entropy ($1/S$) and viral spreading fitness

kendall's rank correlation	kendall tau	p-value	tau 95% CI
Position Entropy vs. Spreading Fitness	-0.256	0.0389	(-0.448 - -0.044)
Position Sensitivity vs Spreading Fitness	-0.381	0.0021	(-0.545 - -0.212)

spearman's rank correlation	spearman rho	p-value	rho 95% CI
Position Entropy vs. Spreading Fitness	-0.379	0.0296	(-0.616 - -0.077)
Position Sensitivity vs Spreading Fitness	-0.558	0.0007	(-0.729 - -0.300)

3.3.5 Conclusions

We use a novel implementation of population genetics framework to translate HIV-1 subtype C database sequences into a fitness landscape. Using this framework, we discovered that the physico-chemical selective forces underlying replicative fitness costs upon mutation varied from

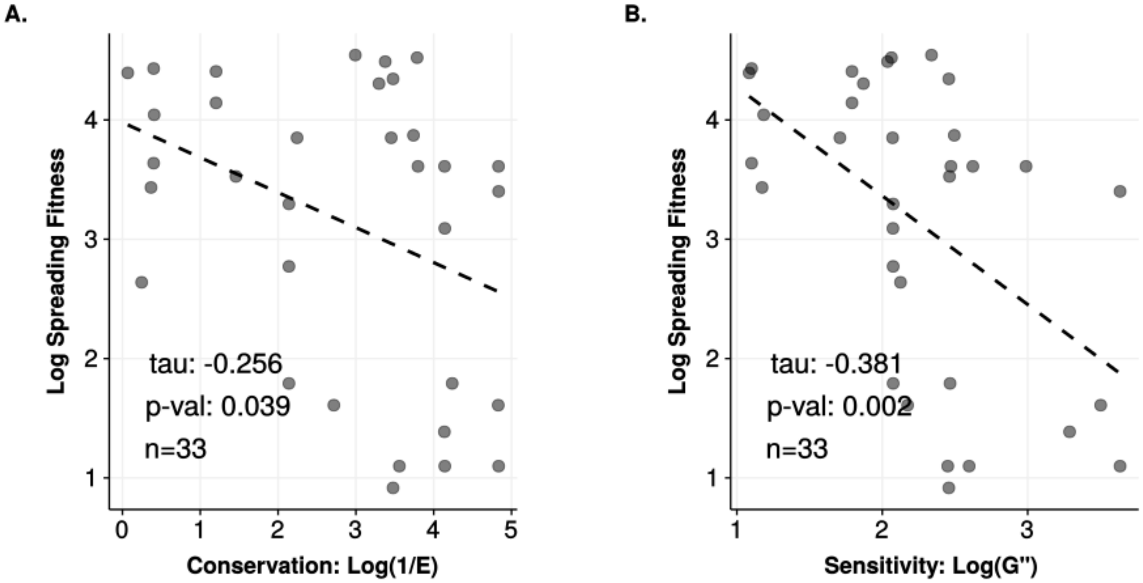

Figure 3.7: Correlation of entropy and sensitivity of residues with the spreading fitness of 31 viral strains bearing mutations in the corresponding residues A) Correlation of the assayed spreading fitness of the mutated virus in days with the correspondingly position's entropy B) Correlation of the assayed spreading fitness of the mutated virus in days with the correspondingly position's physico-chemical sensitivity.

functional region to functional regions. It also became clear that the generative process underlying the distribution of the physico-chemical sensitivities was likely one in which many positive random independent variables were acting proportionally on one another. One biological case in which this might occur is where residues are interacting on eachother (epistasis). It also became clear upon analysis of the distribution of sensitivities that our proxy for fitness cost was not uniform over the poly-protein varying in degree and distribution in different functional regions. Our proxy of fitness cost correlated well with shannon entropy a metric often employed to predict fitness effects in the literature. However, these physico-chemical sensitivities seemed to be a better predictors of the rank order of these fitness effects, both *in vitro* and *in vivo*.

Acknowledgments

We would like to acknowledge the Theoretical Biology and Biophysics Division at Los Alamos National Laboratory for the HIV compendium and alignments made available by their group https://www.hiv.lanl.gov. The HIV Compendia are funded by the Division of AIDS, National Institute of Allergy and Infectious Diseases, through an interagency agreement with the U.S. Department of Energy. This work was supported by a research assistantship offered thorough the National Institute of Mathematical and Biological Synthesis (NIMBioS). NIMBioS is sponsored by the National Science Foundation through NSF Award DBI-1300426, with additional support from The University of Tennessee, Knoxville.

3.4 Supporting information

3.4.1 Physico-chemical weights

Table 3.10: Physico-chemical Weights Weights were extracted via fitting of the model to MSA data for the entire poly-protein (All) and in individual functional regions (p24,p17,p7,p6) The parameters (θ_c, θ_p, θ_v) denote the weighting terms for composition, polarity, and molecular volume respectively

Region	θ_c	θ_p	θ_v	$Log(\mathcal{L})$
All	0.7738	0.22652	0.00047885	-69040
p17	0.77329	0.22628	4.2992e-05	-26456
p24	0.77325	0.22634	0.0004128	-20679
p7	0.77301	0.22613	0.00085456	-5086.3
p6	0.77299	0.22664	0.00036578	-11331

3.4.2 Distribution of Fitness Proxy Metrics

Table 3.11: Null and alternative model describing distribution of physico-chemical sensitivities The distribution can be described using a family of parametrized probability density functions (HA) that describe the distribution in each functional region or this model can be simplified so that the distribution is described by a single Lognormal pdf (H0).

Model H0

Region	PDF	Par(1)	Par(1) value CI 95%	Par(2)	Par(2) value CI 95%
All	Lognormal	sigma	0.705 (0.657,0.759)	mu	1.909 (1.837,1.981)

Model HA

Region	PDF	Par(1)	Par(1) value CI 95%	Par(2)	Par(2) value CI 95%
p17	Lognormal	sigma	0.789 (0.697,0.903)	mu	1.756 (1.610,1.901)
p24	Lognormal	sigma	0.592 (0.534,0.662)	mu	2.150 (2.059,2.241)
p6	Lognormal	sigma	0.685 (0.565,0.855)	mu	1.547 (1.343,1.752)
p7	gamma	alpha	3.792 (2.488,5.509)	beta	0.558 (0.353,0.828)

Table 3.12: Congruity of Descriptive Distributions for Metrics This table displays how the distributions of physico-chemical sensitivities (G") and conservation values ($1/E$) compare over the entire Gag poly-protein (All) and over specific functional regions (p6,p7,p24,p17).

Region	Descriptive PDF (G")	Descriptive PDF (1/E)	Congruous
All	Lognormal	Lognormal	Yes
p17	Lognormal	Lognormal	Yes
p24	Lognormal	gamma	No
p6	Lognormal	inverse gamma	No
p7	gamma	gamma	Yes

3.4.3 Model Comparison

The probability of observing the set of amino acids $\vec{x}$ at a position in a population where they occur at frequency $\vec{p}$ is given by the following multinomial (eq. 3.11).

$$P(\vec{x} \mid \vec{p}) = \frac{\Gamma(\sum_j x_j + 1)}{\prod_j \Gamma(x_j + 1)} \prod_{j=1}^{20} p_j^{x_j} \tag{3.11}$$

Therefore we can express the likelihood of the model given the data as follows (eq. 3.12).

$$\mathcal{L}(\vec{p} \mid \vec{x}) = \frac{\Gamma(\sum_j x_j + 1)}{\prod_j \Gamma(x_j + 1)} \prod_{j=1}^{20} p_j^{x_j} \tag{3.12}$$

The log likelihood of the observed amino acid set $\vec{x}$ for the position now can be written as (eq. 3.13).

$$\ln(\mathcal{L}(\vec{p} \mid \vec{x})) = \ln\left(\frac{\Gamma(\sum_j x_j + 1)}{\prod_j \Gamma(x_j + 1)}\right) + \sum_{j=1}^{20} x_j \ln(p_j) \tag{3.13}$$

The shannon entropy (eq. 3.14) for the position is therefore associated with the log likelihood of observing the set of amino acids $\vec{x}$ in the following way (eqs. 3.15) - 3.18]. In these equations N is the sum of the amino acid counts represented by the vector $\vec{x}$. The shannon entropy calculation assumes that $p_j = \frac{x_j}{N}$.

$$H(\vec{p}) = \sum_{j=1}^{20} p_j \ln\left(\frac{1}{p_j}\right) \tag{3.14}$$

$$\ln(\mathcal{L}(\vec{p} \mid \vec{x})) = \ln\left(\frac{\Gamma(\sum_j x_j + 1)}{\prod_j \Gamma(x_j + 1)}\right) - \sum_{j=1}^{20} x_j \ln(p_j) \tag{3.15}$$

$$-\ln(\mathcal{L}(\vec{p} \mid \vec{x})) = -\ln\left(\frac{\Gamma(\sum_j x_j + 1)}{\prod_j \Gamma(x_j + 1)}\right) - \sum_{j=1}^{20} x_j \ln\left(\frac{1}{p_j}\right) \tag{3.16}$$

$$-\frac{1}{N}\ln(\mathcal{L}(\vec{p} \mid \vec{x})) = -\frac{1}{N}\ln\left(\frac{\Gamma(\sum_j x_j + 1)}{\prod_j \Gamma(x_j + 1)}\right) - \sum_{j=1}^{20} \frac{x_j}{N} \ln\left(\frac{1}{p_j}\right) \tag{3.17}$$

$$-\ln(\mathcal{L}(\vec{p} \mid \vec{x})) = -\ln\left(\frac{\Gamma(\sum_j x_j + 1)}{\prod_j \Gamma(x_j + 1)}\right) - N\sum_{j=1}^{20} p_j \ln\left(\frac{1}{p_j}\right) \tag{3.18}$$

$$-\ln(\mathcal{L}(\vec{p} \mid \vec{x})) = -\ln\left(\frac{\Gamma(\sum_j x_j + 1)}{\prod_j \Gamma(x_j + 1)}\right) - N \cdot H(\vec{p}) \tag{3.19}$$

$$\ln(\mathcal{L}(\vec{p} \mid \vec{x})) = \ln\left(\frac{\Gamma(\sum_j x_j + 1)}{\prod_j \Gamma(x_j + 1)}\right) + N \cdot H(\vec{p}) \tag{3.20}$$

As the number of ways we could have drawn the amino acids increases (1st term) the likelihood increases. However as the shannon entropy increases the likelihood decreases, or as the position becomes more disorganized the probability of drawing any particular set of amino acids decreases. We can thinks of the shannon entropy H as the scaled average number of guesses it takes to identify the correct amino acid at the position given a perfectly organized guessing tree. This value is timed by N the total number of positions observed.

Chapter 4

Mutational Shift of the Gag poly-protein during early and acute infection

Abstract

Our findings suggest HIV structural proteins encoded by the Gag poly-protein do not substantially move closer to the consensus strain over the early stage of infection. This analysis was conducted by examining patient level viral evolution using two distinct measures of fitness. One measure assessed the viral population's likelihood given sequence diversity and the other calculated the Hamming distance of the population from the consensus strain of HIV. Little is understood about HIV fitness during early infection (Arnott et al., 2010); however, one study conducted by Troyer et al. (2005) suggests viral replicative fitness in culture improves over the course of infection. We examined fitness in HIV structural proteins via a patient cohort sampled during the Tshedimoso study Novitsky et al. (2009). On average, 30 positions in the HIV protein Gag transitioned from one type of amino acid residue to another during this study. Given that the Gag polyprotein is highly functionally constrained (Rihn et al., 2013; Miura et al., 2010), we hypothesized that this region would become more fit as the population expanded post the transmission bottleneck (Carlson et al., 2014). Instead, we found that despite the substantial mutation, the net impact of the mutation on the protein appeared to be neutral. This neutrality was most evident in the metric of fitness that accounted for the differential fitness costs of the polymorphisms. It has been suggested, that shed polymorphisms may be balanced out by milder polymorphisms accrued elsewhere in this protein Novitsky et al. (2013). In this way, the overall mutational distance from consensus remains the same. Our results support this idea, given the fitness of the structural elements on a protein level were more static than one might suspect given the number of observed mutations along the protein during this period. The number of populations displaying increased fitness were counterbalanced by populations displaying decreases in fitness. These findings suggest that host immune responses are rather idiosyncratic in their ability to depress fitness in viral structural proteins, if they can at all.

4.1 Introduction

The Gag polyprotein is an important immune target. Its functionally and structurally constrained cleavage products comprise over 50 % of the viral mass (Waheed and Freed, 2012; Li et al., 2010). Elite controllers are patients who are able to control their HIV viral load. Elite controllers often target critical epitopes within this region of the polyprotein, leading to successful and sustained control over the virus (Honeyborne et al., 2007; Rolland et al., 2008). Consequently, HIV vaccines typically incorporate immunogens from this region in their constructs (Li et al., 2010; Waheed and Freed, 2012; Goulder and Watkins, 2004; Korber et al., 2009).

The first year of viral evolution is particularly critical in determining patient outcomes. There is a well-established relationship between disease progression and viral fitness (Quiones-Mateu et al., 2000). By the first year, the viral load's set point for the chronic infection is well established. This fitness setpoint is often predictive of when the patient will progress to AIDS (**?**). The majority of evolution occurs during this first year as well, prior CD4 T-Cell decline (Li et al., 2007) . During this period, the virus still enjoys an abundance of target cells and immune responses have not yet been severely compromised. We wished to assess whether the transiently potent CTL response managed to depress viral fitness during this critical period. Other assessments of viral fitness (Troyer et al., 2005) have suggested *in vitro* replicative fitness of the virus increases over time. Likewise, others have shown that the virus rapidly sheds unfit polymorphisms acquired in the previous host (Carlson et al., 2014). By shed we mean that these non-consensus residues disapear from the population. We may also expect viral fitness to increase due to the adaptive expansion the virus is undergoing after a tightly bottlenecked transmission event. By bottleneck, we mean that viral infection is only founded by a few viruses that are biased towards being consensus like in nature due to the mechanics and biology of transmisson (Carlson et al., 2014).

One approach to designing a vaccine immunogen is to prime host immune responses to push the virus over its error threshold Korber et al. (2009); Tripathi et al. (2012); **?**. This is accomplished by designing immunogens that elicit immune responses against a broad set of mutationally fragile regions. Given this approach, we wanted to see if natural unprimed host immune responses were already managing to depress viral structural fitness to any appreciable degree. Ideally, successful natural responses could be strengthened by exposure to a vaccine immunogen. Studies have suggested that the Gag poly-protein is tightly co-linked epistatically (Dahirel et al., 2011), with compensating mutations rapidly arising whenever a deleterious mutation arises in the region due to CTL pressure (Brockman et al., 2010, 2007; Burwitz et al., 2011). Therefore, it may be difficult to depress viral fitness in this regions, much less force it over its error threshold.

Little is understood about how viral fitness changes during the early stages of infection. To establish whether the viral structural elements were increasing or decreasing in fitness, we assessed fitness trends in 41 HIV-1 subtype C infected 41 patients. Changes in the viral population structure were captured using two different metrics. In the first approach, we employed a standard Hamming distance metric that calculated population distance from the HIV consensus stain. In the second approach, we employed a polymorphism sensitive likelihood measure which determined the likelihood of the viral contents of a blood sample given global subtype diversity.

4.2 Methods

4.2.1 Sequences

Longitudnal Sequences

The HIV-1 Gag sequences used to construct the viral population kinetics in this analysis, came from a primary HIV-1 subtype C infection study conducted in Botswana from 2004-2005 (Novitsky et al., 2011, 2009). In this study, a cohort of 42 HIV-1 subtype C positive individuals had their blood drawn at 4-6 points in a 500 day period after sero-converting. Patients were newly infected.

Of the 42 patients, 34 individuals were in Fiebig stage IV or V (20-100 days post infection) the other 8 were still in Feibig II (˜15-20 days post infection). It was impossible to get a linear fit for Patient "OM" individually because the patient had only two recorded blood samples. Therefore patient "OM" is omitted from the sample in the patient breakdowns.

Cross-sectional Sequences

We use 1058 curated sequences in the Los Alamos database for subtype C (2016) (see Los Alamos HIV-1 Sequence Database). These sequences were filtered web alignments that provide a good example of the subtypes breadth. Every sequence belongs to a unique patient and sequences that resemble each other too closely had been removed. This was to make sure duplicate sequences were not used. Additionally questionable sequences such as those that appear to be hypermutants and synthetics have also been removed. The curated sequences were clean, containing little amibuous coding, few long insertions and lacked a preponderance of frame shifts. Sequences in this curated alignment were aligned using both automation (HMMER) and manual editing.

4.2.2 Calculating the Fitness of Patient Viral Populations via Hamming Distances

We describe the intrinsic fitness (F) of the virus in the blood sample (X_t) taken from the patient at time t in terms of viral Hamming distance from the viral consensus (eq. 4.1). This measure of sequence mutation which treats sequences as binary strings (0 non-deviation from consensus, 1 deviation from consensus) if often employed to infer viral fitness and estimate viral diversity Ferguson et al. (2013); Pilcher et al. (2008). In this context, we define the hamming distance as the residue distance between the sampled viral sequence and the HIV-1 subtype C consensus sequence (see Los Alamos Consensus Alignment Database).

$$F(X_t) = \frac{\sum_j^s \sum_i^n \delta_\mu(r_{ij})}{\sum_j^s \sum_i^n \delta(r_{ij})}. \tag{4.1}$$

$$\delta_\mu(r_{ij}) = \begin{cases} 1, & \text{if } \hat{p}(r_{ij}) < \hat{p}_{max} \\ 0, & \text{if } r_{ij} \in \{-,*\} \\ 0, & \text{otherwise} \end{cases} \tag{4.2}$$

Each element r_{ij} in the HXB2 residue vector $\vec{r_j}$ of length n represents the state (residue, gap, stop codon) at HXB2 coordinate position i in viral sequence j. We use two Kronecker delta functions (δ_μ, δ) to count the total number of HXB2 coordinates bearing mutations δ_{mu} (eq. 4.2) and the total number of HXB2 coordinates bearing one of the 20 natural amino acid residues δ (eq. 4.3). Because we are defining hamming distance in terms of residue differences, residue coordinates containing gaps or stop and start codons $\{-,*\}$ are ignored in both Kronecker delta counts. Mutations are defined in the Kronecker delta function (δ_μ using prevalence map which recorded the prevalence of each coordinate state $\hat{p}(r_{ij})$ for a 1058 sequence sample taken from curated alignment for HIV subtype C www.hiv.lanl.gov.The prevalence map was augmented to account for non-observed residues, with the prevalence set at $1/1058$ or 0.000945 for non-observed residues. The Kronecker delta function δ_μ can either categorize a mutation conservatively or permissively. Using the conservative definition, a residue coordinate will be classified as mutated if the the residue it bears at that position has a prevalence of less than 0.50. In this way, any residue at a highly polymorphic position will be automatically classed as mutated and only fitness shifts at conserved positions will be monitored. Using a more permissive definition, the Kronecker delta function will classify anything that has a prevalence lower than that of the consensus residue as mutated.

$$\delta(r_{ij}) = \begin{cases} 0, & \text{if} \quad r_{ij} \in \{-, *\} \\ 1, & \text{otherwise} \end{cases} \tag{4.3}$$

$$\hat{p}_{max} = \begin{cases} 0.50, & \text{if conservative} \\ \hat{p}(r_{ic}), & \text{if permissive} \end{cases} \tag{4.4}$$

4.2.3 Estimating the Fitness of Patient Viral Populations from Global Population Likelihoods

Each set of viral variants sequenced from a patient's blood sample is regarded as representative of the larger viral population in the blood compartment. The total number of residues observed at any HXB2 coordinate j in the blood sample is n_j. The values $x_{1,j}...x_{20,j}$ represent the counts for each of the 20 natural amino acids. The value $\hat{p}(a_{ij})$ denotes the prevalence of that amino acid i at the sequence coordinate position.

$$\mathcal{L}(\theta_{\hat{p}} \mid X_t) = \prod_{j=1}^{520} \left(\frac{n_j!}{x_{1,j}! \cdots x_{20,j}!} \prod_{i=1}^{20} \hat{p}(a_{ij})^{x_{ij}} \right) \tag{4.5}$$

j in the database. In this way we can can calculate the likelihood of sequencing a particular set of amino acids for a position from a blood sample. By multiplying these likelihoods over the length of the sequence. we can calculate the probability of drawing the provided blood sample (X_t) given what we know about the prevalence of residues in the larger circulating population of virus ($\theta_{\hat{p}}$). So every likelihood multiplied is the probability of observing the amino acid distribution we found at that position.

4.2.4 Statistics On Fitness Trends

Two marginal homogeneity tests were conducted to determine if the method used to estimate fitness impacted categorization of the patients. The tests evaluated a null hypothesis where both metrics are assumed to categorize the mutational trajectory of the patients viral populations similarly. Patient viral populations were either categorized as increasing in fitness or descreasing linear regression. A contingency table was constructed where an increasing or descreasing trend was regarded as a dichotomous viral population trait. The method used to estimating fitness was considered the treatment for our viral populations. Marginal homegeneity of the differences in the viral population classifications was assessed using both a standard McNemar Chi-squared Test and Bhapkar Marginal Homogeneity Test given that is was a good extension of the Stuart-Maxwell test with more power (Agresti, 2003).

To insure that the polymorphic fitness trends we identified were not false positives, we assessed the robustness of the polymorphic fitness trends via bootstrapping . Sequence sets amplified from each blood sample were re-sampled 1000 times at each time-point to create 1000 re-sampled mutational trajectories for each patient. Linear fits were conducted for all re-sampled trajectories, from the distribution of resulting slopes with p-values the robustness of the detected shift was calculated by dividing the number of re-sample trajectories showing a significant shift in mutational character over the total number of trajectories.

Method specific viral populations fitness trends were assessed with a linear regression. Estimates of viral population fitness were generated from patient blood samples taken up to 700 days post-seroconversion. Regressions of trends were displayed with confidence bands denoting the standard error of respective regression. We begin by assuming there is no trend in the viral population, and the slope of our regression is zero. The p-value we obtain represents the probability of recording a slope that is as extreme or more extreme than the one we observed (assuming there really is no trend). If we obtain a slope with a p-value of 0.02, this means that if we were to resample the patient 100 times and rerun our regression, we would obtain a slope as extreme as this (or more) 2 out of every 100 resamples. This 2% chance of obtaining a false positive by random chance seems small, so we reject the notion that the null hypothesis is true and consider the alternate hypothesis that the trend is real. Most of the time we want the probability of obtaining a false positive (the type I error) to be below 5%. However, in some cases, we desire it to be lower because we are running more experiments. Our chance of obtaining a false positive due to random error increases as we look for viral population trends in more patients. We therefore run a BenjaminiHochberg procedure with our False Discovery Rate set at a tolerance of 25%. Patients whose viral trends remained significant are noted with asterisk.

4.3 Results

4.3.1 Polymorphic Approach: HIV Structural Proteins Show No Discernible Trend of Increased Fitness Over Acute Infection

Figure (4.1) displays breakdowns of mutational trajectories by method. A Polymorphic, Permissive and Conservative method were used to comparatively assess how a patient's viral population evolved. Specifically, the goal was to assess if a patient's viral population became 1) more fit 2) less fit or 3) remained static over the acute infection period. Panels in Figure (4.1) display the break down of viral evolution in the patient cohort by method. The viral sequences sampled from 41 HIV-C acutely infected patients (4-12 timepoints), were used in the fitness calculations.

The fitness status of the current viral population was evaluated per timepoints using all three methods (Polymorphic, Permissive, Conservative) and resulting trends were identified via regression. In the polymorphic classification scheme, viral population fitness was interpreted in terms of how likely one was to draw that particular blood sample given the diversity of database sequences. (eq 4.1). In the permissive classification scheme, any non-consensus residue was

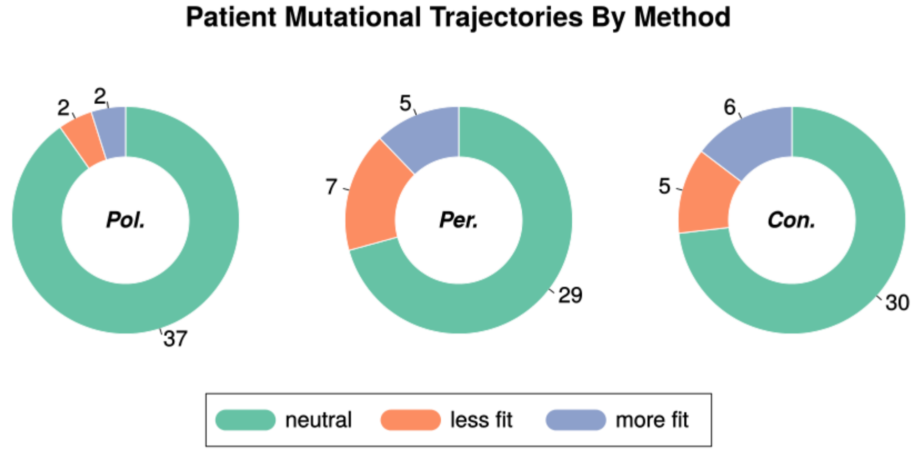

Figure 4.1: Comparative Assessment of Viral Evolution Polymorphic, Permissive and Conservative methods comparatively assess viral population fitness shifts over 4-12 time points. Panels display categorization of fitness shifts (neutral,less fit,more fit) in acutely infected patient cohort (41) by method. **Pol.** Polymorphic Classification Scheme gives likelihood of drawing a particular blood sample given the diversity of database sequences(eq 4.5). **Per.** Permissive Classification Scheme, where non-consensus residues categorized as unfit. (eq 4.1). **Con.** Conservative Classification Scheme, where highly polymorphic sites (consensus frequency $\leq 50\%$) effectively disregarded (eq 4.1).

.

categorized as unfit. This rather binary estimate of fitness was overly liberal in classifying mutations given that positions in this poly-protein can bear more than one dominant residue (eq 4.1). In the conservative classification scheme, the metric used to categorize mutations was conservative as to what was categorized as a mutation with changes at highly polymorphic sites (consensus frequency $\leq 50\%$) being effectively disregarded (eq 4.5).

The polymorphic method of assessing fitness trends detected little to no change in the fitness status of the virus over acute infection (Fig 4.5). The other two hamming based methods were more liberal in their classification of mutations and did detected more fitness shifts in the patient cohort. However, at a patient population level, the shifts in fitness followed no discernible pattern. Some patient viral population's became more fit in regards to their structural elements, while an approximately equal number declined in fitness. Shifts were not detectable in pooled blood sample estimates given the patient heterogeneity (Fig A-B S.4.5) for the conservative and permissive measures of fitness. A shift towards fitness was detected using the polymorphic approach on the pooled samples. However, given that this positive trend does not carry over at the patient level, it is likely an artifact of pooling the data (Figure C S.4.5).

4.3.2 Classification of Mutational Trends

Figure (4.2) displays how intra-host viral populations evolved over acute infection using three different approaches to appraise fitness, two in which hamming distance from the consensus sequence was used as a measure of fitness (Permissive,Conservative) and one in which a likelihood measure was used to estimate fitness (Polymorphic).

Each point on the graphs represents a method specific estimate of viral population fitness at some time-point post-seroconversion. Each fitness estimate was calculated using either the simple permissive and conservative hamming distance measures or the more complex polymorphic measure that was based on the likelihood of drawing the blood sample. The left column presents the patients which showed a significant increase in fitness, the right columns the patients who

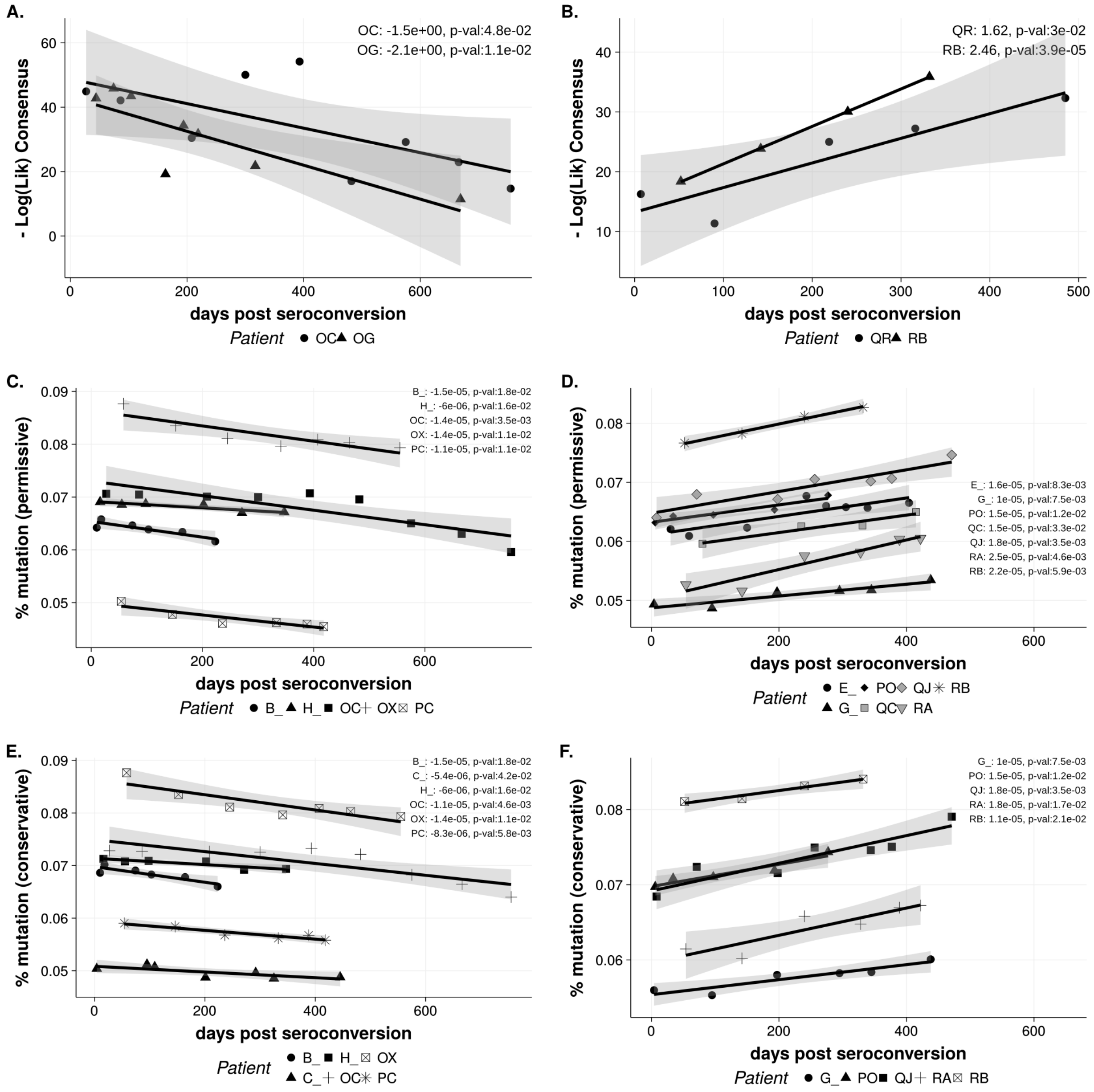

Figure 4.2: Method Specific Viral Populations Fitness Trends Each point represents a method specific estimate of viral population fitness from a patient blood sample taken up to 700 days post-seroconversion. A cross-sectional viral sample (n=5-30) was amplified via SGA from each blood draw (Novitsky et al., 2009). Left panel displays patients showing a significant increase in fitness, right panel patients showing a significant decrease. Trend lines generated via linear regression with confidence bands denoting standard error of respective regressions. **A-B.** Polymorphic classification scheme, y-axis denotes fitness in terms of viral sample likelihood (eq 4.5). **C-D.** Conservative classification scheme, y-axis denotes fitness in terms of percent of unfit residue in blood sample. Residue substitutions at highly polymorphic sites (consensus frequency $\leq$ 50%) disregarded (eq 4.1). **E-F.** Permissive classification scheme, y-axis denotes fitness in terms of percent of unfit residues in blood sample with non-consensus residues categorized as unfit (eq 4.1).

showed a significant decrease in fitness. In the polymorphic classification scheme, viral population fitness was interpreted in terms of how likely one was to draw that particular blood sample given the diversity of database sequences. (eq 4.1). Therefore, counter intuitively, as the $-Log(\mathcal{L})$ value of the blood sample decreases the virus becomes more fit and as the $-Log(\mathcal{L})$ value increases the virus becomes less fit. (Fig. 4.2.A-B) In the permissive classification scheme, any non-consensus residue was categorized as unfit (eq 4.1).The total number of unfit sampled residues out of total number of sampled residues is reported on the y-axis (Fig. 4.2.C-D). In the conservative classification scheme, changes at highly polymorphic sites (consensus frequency $\leq$ 50%) were not used to track fitness (eq 4.5) so that polymorphisms would not be mistakenly factored in as as unfit residues. Likewise, the total resulting number of unfit sampled residues out of total number of sampled residues is reported on the y-axis (Fig. 4.2.E-F).

From Figure 4.2 we can observe that the hamming distance methods that failed to take polymorphisms into account (conservative) or only partially took polymorphisms into account (permissive) consequently identified many more putative viral population shifts. The method that took polymorphism into account, however, only identified two patients in which the viral population became substantially less fit and two where there was an increased in fitness. Notably, patient QR was classified as decreasing in fitness in the polymorphic method but not in the hamming distance measures which failed to detect any shift. Likewise, OG was only found to be increasing in fitness using the approach that acknowledged polymorphisms.

Table 4.1 displays the results of two marginal homogeneity tests demonstrating that a polymorphic approach to assessing fitness trends results in a different categorization of patients compared to a permissive classification approach. Both the Bhapkar and McNemar Chi-squared marginal homogeneity tests evaluate a null hypothesis where both approaches are assumed to categorize the mutational trajectory of the patient's viral populations similarly.

Table 4.1: Conservative and Permissive Metric vs Polymorphic Metric Two marginal homegeneity tests were conducted to determine if metric type impacted categorization of the patients. The tests evaluated a null hypothesis where both metrics are assumed to categorize the mutational trajectory of the patient's viral populations similarly.

Conservative vs Polymorphic	χ^2	**p-val**
McNemar's Chi-squared Test	3.27	0.0704
Bhapkar Marinal Homogeneity Test	5.01	0.0816

Permissive vs Polymorphic	χ^2	**p-val**
McNemar's Chi-squared Test	4.08	0.0433
Bhapkar Marinal Homogeneity Test	6.18	0.0455

4.3.3 Robustness of Detected Population Shifts

The sequence data employed to estimate the fitness trend lines was uneven in sampling depth with successful single genome amplifications varying from 5 to 30 sequences per blood sample. Given the 1) sampling noise and the 2) qualitatively different polymorphic populations shifts characterized with the polymorphic method, we wanted to ensure the shifts detected using this method were not false positives.

To address this concern, viral sequences were bootstrapped 1000 times per patient blood sample allowing the construction of new time-courses from recalculated fitness estimates. Regressions were then run all 1000 new patient time-courses and significant and non-significant trends were recorded (Fig.4.4).

Using this approach, the robustness of the detected shift was estimated by dividing the number of re-sample trajectories showing a significant shift in fitness over the total number of trajectories. This empirical bootstrap demonstrated that all populations shifts were robust under resampling except in Patient OC (Table 4.2). Given these results, we can assume the qualitatively different shifts observed with the polymorphic method were not an artifact of sampling noise but genuine shifts in the character of the population over early infection.

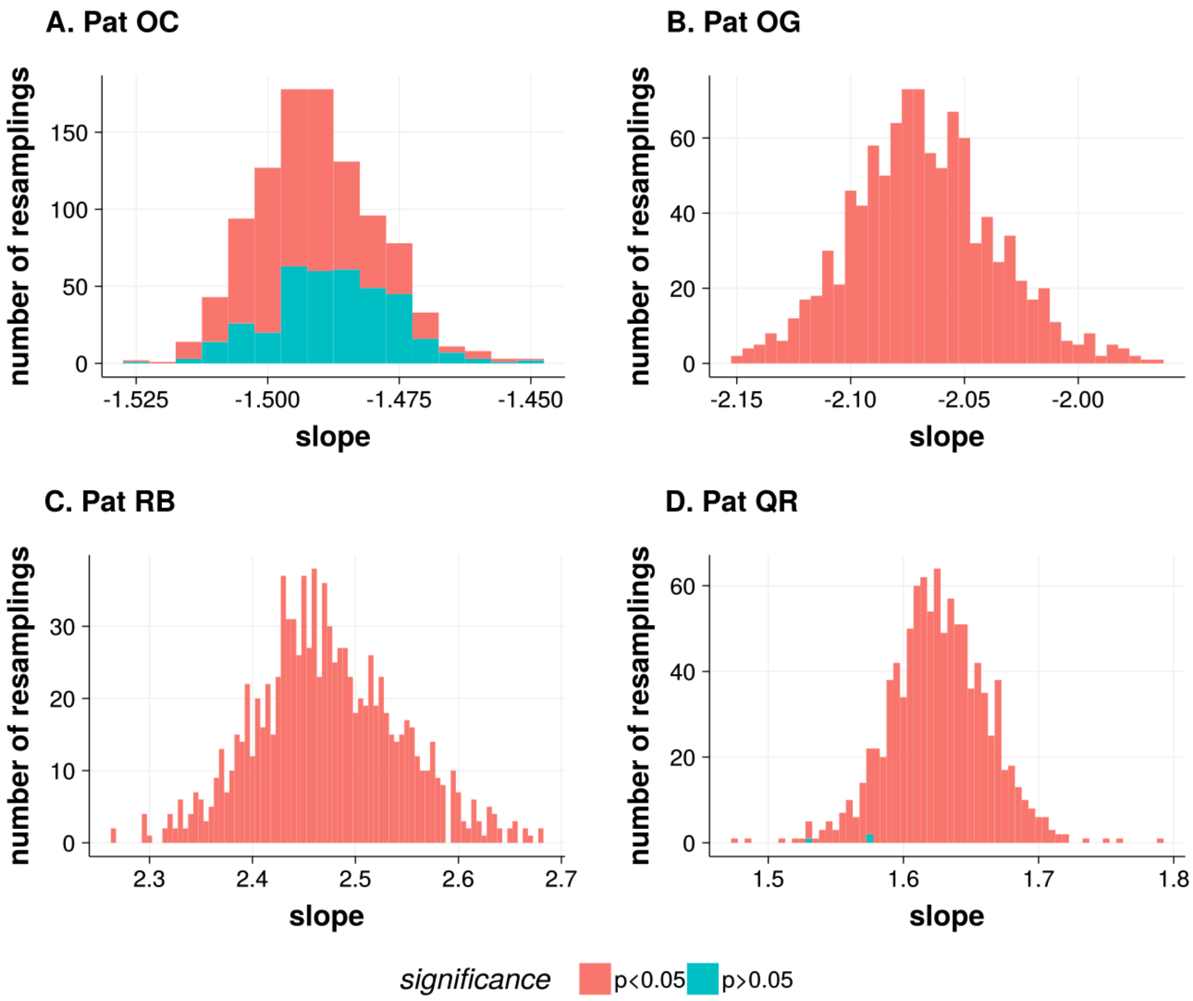

Figure 4.3: Empirical Bootstrap of Viral Sequences Robustness of the four patients shifts for the Polymorphic metric assessed by bootstrapping (n=1000) the patient blood samples. Post bootstrapping, polymorphic fitness estimates were recalculated. Slopes from linear regressions on the newly constructed time-courses were categorized as significant or non-significant. Panels displays the distribution of slopes obtained from each of the four patients. Colors denote the significant and non-significant slopes in the empirical bootstrap.

Table 4.2: Robustness of Detected Population Shifts The sequence sets amplified from each blood sample were re-sampled 1000 times at each time-point to create 1000 re-sampled mutational trajectories for each patient. Linear fits were conducted for all re-sampled trajectories, from the distribution of resulting slopes with p-values the robustness of the detected shift was calculated by dividing the number of re-sample trajectories showing a significant shift in mutational character over the total number of trajectories.

Patient	Trend	Robustness	Population Shift $[Log(\mathcal{L})/\text{day}]$
QR	Less Fit	0.997	1.626
RB	Less Fit	1.000	2.468
OC	More Fit	0.629	-1.491
OG	More Fit	1.000	-2.0669

4.4 Discussion

4.4.1 Polymorphic Approach: Expected Fitness Increase in Viral Structural Elements Not Observed

The expected increase in the fitness of the viral structural elements was not observed for most of these patients (Figure 4.1). We expected to observe this increase given that *in vitro* fitness assays of patient virus show an increase in the over-all fitness of the virus over infection (Troyer et al., 2005). Additionally, this region of the HIV-1 genome is believed to be under rather unforgiving structural and functional purifying pressures (Abidi et al., 2014; Rihn et al., 2013). Taken together, this suggested the viral structural elements encoded by Gag would trend towards becoming more fit during this period as the virus fine tuned its intra-host fitness post the transmission bottle-neck.

Counter to our expectations, the fitness of the structural elements rarely increased over the course of acute infection. In addition many patients experienced a decrease in the fitness of their structural elements (Figure 4.2). These results could be indicative of two scenarios. On the one hand, overall viral fitness trends, may not be reflective of the fitness trends of viral structural elements. Alternatively, these results may indicate that *in vitro* fitness assays are failing to capture critical aspects of *in vivo* fitness. One pitfall in competitive replication assays, is they can only assess viral fitness in regards to infectivity and replication. In addition, they are biased towards measuring these aspects of fitness on particular subsets of cells. Other critical aspects of fitness are not captured, these including viral resilience to innate and adaptive host immune pressures and migratory capability. The failure of fitness trends in the Gag poly-protein to correspond to overall viral trends may be due to the fact that the Gag-polyprotein experiences an unforgiving degree of purifying pressure compared to other viral protein (Abidi et al., 2014; Rihn et al., 2013). Due to this pressure, forward mutations (unfit mutations) must be compensated by reversions (fit mutations) elsewhere on the poly-protein. On a protein level, therefore, the protein's fitness status may remain static over the acute period despite the extensive degree of evolution at the residue level (+30 residues mutations per 520). Supporting this idea, it has been observed that 1) Gag forward mutations early in infection are quickly followed and balanced by reversions in the poly-protein (Li et al., 2007; Novitsky et al., 2013). The Gag poly-protein possesses identifiable sets of residues that seem to co-evolve together (Dahirel et al., 2011). Additionally, compensating pathways have been mapped for particular CTL epitope targets (Burwitz et al., 2011; Koek et al., 2012; Rolland et al., 2010). Our results suggest that heavy CTL targeting does not substantially decrease the overall fitness of the viral structural components during a natural acute infection. This is a disheartening result given that eliciting CTL targeting of Gag immunogens is an foundational strategy for many HIV vaccines (Walker and Burton, 2008; Korber et al., 2009). On the other hand, Gag derived proteins do not appear to greatly increase in fitness over the acute period either. This suggests that the virus may be occupynig a rather narrow fitness zone representing a riposte between purifying pressure and immune pressure and that this fitness zone remains rather stable over acute infection.

4.4.2 Adding Biological Detail Produced Qualitatively Different Trends

It was not clear if the added biological detail of accounting for polymorphims would significantly change the way we described viral fitness shifts. To explore this impact, two marginal homogeneity test were conducted on patient categorizations resulting from conservative (non-polymorphic) and polymorphic approaches. These tests allowed us to assess whether the conservative and polymorphic approaches similarly classified viral population behavior. Both tests suggested, the approaches were not classifying viral trends similarly. Taking into account polymorphism appeared to fundamentally changes the putative viral fitness trends observed. Given these findings, as well as the well acknowledged highly diverse mutant spectrum's within hosts (Pennings et al., 2014; Korber et al., 2001), we suggest that future models assessing *in vivo* fitness of virus factor polymorphisms into their fitness assessments.

4.4.3 Further Work

More work should be done to assess viral mutational trends in the other HIV proteins. We might fail to observe any trend towards fitness in these proteins as well. If we did, it would suggest that the *in vitro* and *in vivo* database methods actually predict different evolutionary trajectories not just for the structural elements but for all proteins. This would indicate that these *in vitro* assays may not be capturing critical aspects of viral fitness.

Acknowledgments

We would like to acknowledge the Theoretical Biology and Biophysics Division at Los Alamos National Laboratory for the HIV compendium and alignments made available by their group https://www.hiv.lanl.gov. The HIV Compendia are funded by the Division of AIDS, National Institute of Allergy and Infectious Diseases, through an interagency agreement with the U.S. Department of Energy.

4.5 Supporting information

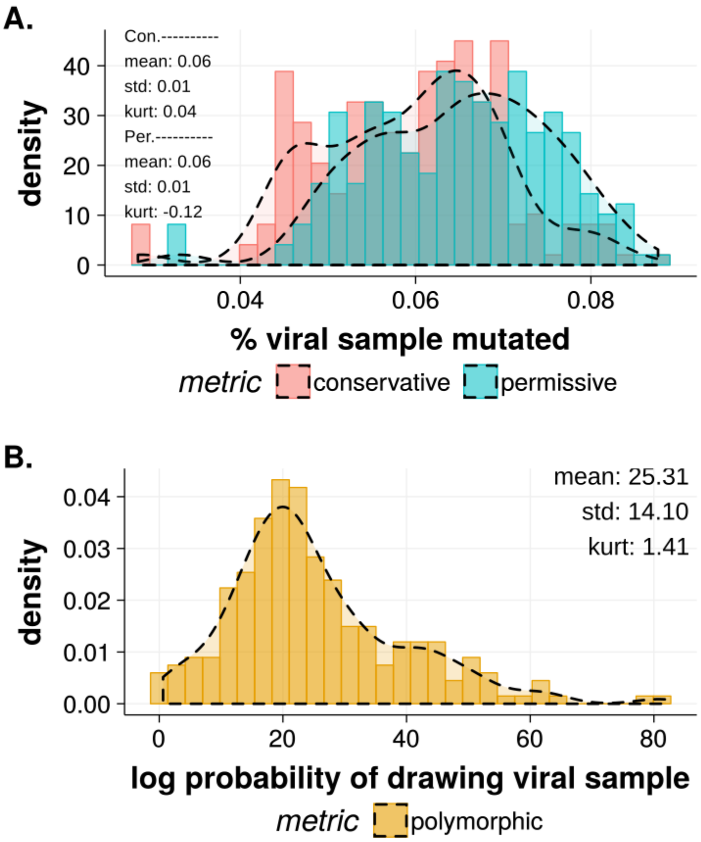

Figure 4.4: Density Plots of Fitness Metrics for Three Approaches. Pooled samples from 41 patients A Permissive and Conservative Metric Density Plot **B** Polymorphic Density Plot. Pooled samples from 41 patients.

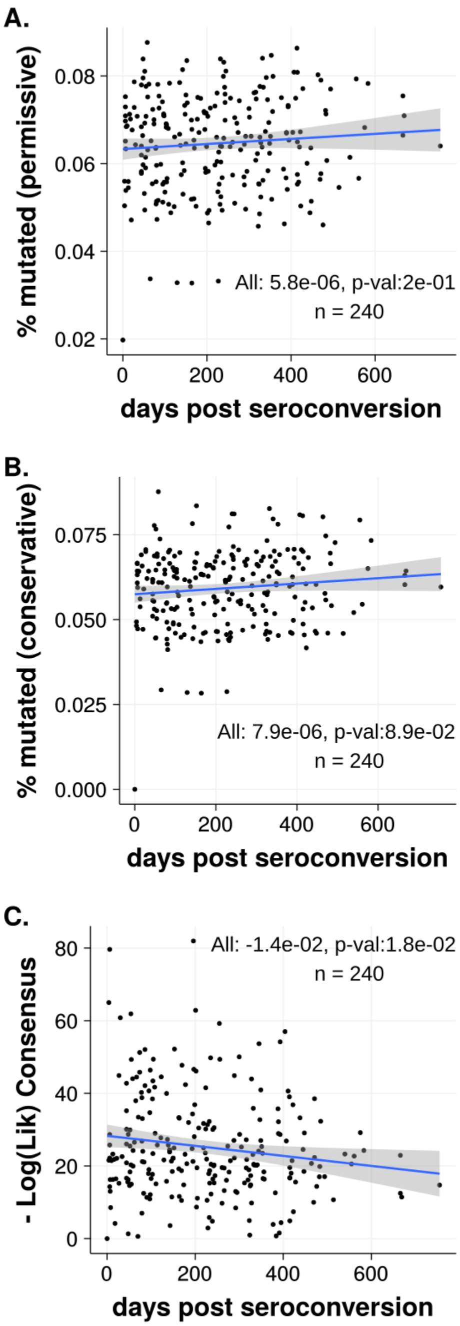

Figure 4.5: Method Specific Viral Population Fitness Trends Only significantly trending patients shown (not FDR corrected). Regression non-weighted, sample size corrected by bootstrapping for adjusted metric. **A.** Permissive classification scheme, y-axis denotes fitness in terms of percent of unfit residues in blood sample with non-consensus residues categorized as unfit (eq 4.1). **B.** Conservative classification scheme, y-axis denotes fitness in terms of percent of unfit residue in blood sample. Residue substitutions at highly polymorphic sites (consensus frequency $\leq$ 50%) disregarded (eq 4.1). **C.** Polymorphic classification scheme, y-axis denotes fitness in terms of viral sample likelihood (eq 4.5).

Table 4.3: Linear fits Polymorphic. False Discovery Rate (FDR) set at 0.25%.

Patient	slope	intercept	R^2	p-val slope	$(i/m)Q$
RB*	2.46	630	1	3.90E-005	0.006097561
OG*	-2.07	1730	0.689	0.0108	0.012195122
QR*	1.62	559	0.834	0.0304	0.0182926829
OC*	-1.5	1950	0.45	0.0478	0.0243902439
OQ*	-1.56	1220	0.736	0.0627	0.0304878049
PA*	-6.86	1850	0.866	0.0694	0.0365853659
OJ*	-1.79	1700	0.703	0.076	0.0426829268
C*	-3.64	2210	0.441	0.104	0.0487804878
OZ	-2.51	1750	0.432	0.109	0.0548780488
RA	1.99	658	0.485	0.124	0.0609756098
OX	-1.26	1420	0.399	0.128	0.0670731707
PD	-0.455	919	0.491	0.188	0.0731707317
OY	-1.2	850	0.268	0.189	0.0792682927
OE	-2.18	1200	0.453	0.213	0.0853658537
D	-2.55	1840	0.25	0.253	0.0914634146
PC	-2.67	1850	0.287	0.273	0.0975609756
OW	-1.75	1420	0.268	0.293	0.1036585366
OS	-1.08	1550	0.15	0.391	0.1097560976
F	0.512	316	0.122	0.442	0.1158536585
G	1.53	911	0.15	0.448	0.1219512195
QT	1.1	1040	0.186	0.468	0.1280487805
QI	-0.681	781	0.158	0.508	0.1341463415
O1	-0.828	1050	0.146	0.525	0.1402439024
QU	-0.973	991	0.192	0.561	0.1463414634
QA	-0.91	1490	0.103	0.599	0.1524390244
NN	-0.804	1200	0.0984	0.607	0.1585365854
B	1.99	970	0.0685	0.616	0.1646341463
H	-1.11	1610	0.0673	0.619	0.1707317073
PP	1.29	777	0.13	0.64	0.1768292683
QP	0.498	1120	0.0983	0.686	0.1829268293
QJ	0.639	925	0.0284	0.718	0.1890243902
QM	0.401	493	0.0648	0.745	0.1951219512
QS	0.483	458	0.0349	0.763	0.2012195122
OU	-0.498	1480	0.015	0.772	0.2073170732
QC	-0.888	1360	0.0473	0.782	0.2134146341
E	-0.511	1380	0.0101	0.813	0.2195121951
A	-0.167	734	0.00491	0.848	0.2256097561
QD	-0.538	1590	0.0135	0.884	0.2317073171
QG	-0.0462	184	0.00532	0.907	0.237804878
PO	-0.136	832	0.0051	0.909	0.243902439

Table 4.4: Linear fits Conservative metric. False Discovery Rate (FDR) set at 25%.

Patient	slope	intercept	R^2	p-val slope	$(i/m)Q$
QJ*	1.84E-005	0.0692	0.843	0.00352	0.006097561
OC*	-1.13E-005	0.0749	0.706	0.00455	0.012195122
PC*	-8.35E-006	0.0594	0.879	0.00578	0.0182926829
G*	1.00E-005	0.0554	0.862	0.00751	0.0243902439
OX*	-1.45E-005	0.0864	0.756	0.011	0.0304878049
PO*	1.47E-005	0.0698	0.909	0.0119	0.0365853659
H*	-6.01E-006	0.0714	0.799	0.0163	0.0426829268
RA*	1.81E-005	0.0596	0.797	0.0167	0.0487804878
B	-1.48E-005	0.0698	0.791	0.0177	0.0548780488
RB	1.14E-005	0.0803	0.957	0.0215	0.0609756098
C	-5.41E-006	0.0508	0.597	0.0416	0.0670731707
E	1.13E-005	0.0637	0.491	0.0527	0.0731707317
QA	5.65E-006	0.0653	0.728	0.0659	0.0792682927
QC	1.53E-005	0.059	0.86	0.0726	0.0853658537
PD	6.02E-006	0.0751	0.694	0.0796	0.0914634146
QI	-2.54E-006	0.047	0.689	0.0818	0.0975609756
OJ	-4.43E-006	0.0781	0.67	0.0904	0.1036585366
QS	7.04E-006	0.0636	0.565	0.143	0.1097560976
QR	1.13E-005	0.0564	0.544	0.155	0.1158536585
QT	7.15E-006	0.0621	0.532	0.162	0.1219512195
QM	2.76E-006	0.0793	0.661	0.187	0.1280487805
QP	5.77E-006	0.0832	0.646	0.197	0.1341463415
QG	-8.48E-006	0.0582	0.474	0.199	0.1402439024
D	3.85E-006	0.07	0.299	0.204	0.1463414634
OQ	-2.04E-005	0.0661	0.366	0.28	0.1524390244
PP	-2.49E-005	0.0576	0.514	0.283	0.1585365854
OG	4.39E-006	0.07	0.165	0.318	0.1646341463
PK	7.59E-006	0.0663	0.34	0.417	0.1707317073
A	-9.44E-006	0.0751	0.0753	0.443	0.1768292683
OW	4.61E-006	0.0562	0.142	0.461	0.1829268293
PA	-3.19E-006	0.0336	0.24	0.51	0.1890243902
NN	1.41E-006	0.051	0.123	0.563	0.1951219512
OS	2.36E-006	0.0758	0.0671	0.575	0.2012195122
OY	1.74E-006	0.0522	0.046	0.61	0.2073170732
OU	2.37E-006	0.0569	0.042	0.626	0.2134146341
OE	4.01E-006	0.0486	0.0849	0.634	0.2195121951
OZ	-2.05E-006	0.0646	0.0393	0.67	0.2256097561
QD	1.87E-007	0.0638	0.107	0.673	0.2317073171
O1	1.84E-006	0.0746	0.061	0.689	0.237804878
F	3.83E-006	0.0577	0.0272	0.724	0.243902439

Table 4.5: Linear Fits Permissive metric. The False Discovery Rate (FDR) tolerance set 25%.

Patient	slope	intercept	R^2	p-val slope	$(i/m)Q$
OC *	-1.37E-005	0.073	0.726	0.00352	0.006097561
QJ *	1.84E-005	0.0648	0.843	0.00352	0.012195122
RA *	2.50E-005	0.0502	0.891	0.00464	0.0182926829
RB *	2.24E-005	0.0754	0.988	0.00587	0.0243902439
G*	1.00E-005	0.0487	0.862	0.00748	0.0304878049
E*	1.56E-005	0.0611	0.714	0.0083	0.0365853659
OX*	-1.45E-005	0.0864	0.756	0.011	0.0426829268
PC*	-1.14E-005	0.05	0.83	0.0115	0.0487804878
PO	1.47E-005	0.0632	0.909	0.0119	0.0548780488
H	-6.01E-006	0.0692	0.799	0.0163	0.0609756098
B	-1.49E-005	0.0654	0.79	0.0178	0.0670731707
QC	1.48E-005	0.0585	0.935	0.0328	0.0731707317
C	-4.97E-006	0.0487	0.513	0.0701	0.0792682927
PD	6.02E-006	0.0663	0.694	0.0796	0.0853658537
QI	-2.54E-006	0.047	0.689	0.0818	0.0914634146
QA	5.11E-006	0.061	0.658	0.0955	0.0975609756
QS	6.30E-006	0.0615	0.559	0.146	0.1036585366
OJ	-1.34E-006	0.0614	0.553	0.15	0.1097560976
QR	1.13E-005	0.0498	0.544	0.155	0.1158536585
QT	7.15E-006	0.0576	0.531	0.162	0.1219512195
QM	2.76E-006	0.0685	0.661	0.187	0.1280487805
QG	-8.48E-006	0.0515	0.474	0.199	0.1341463415
PP	-3.02E-005	0.0505	0.555	0.255	0.1402439024
OQ	-2.00E-005	0.0615	0.363	0.282	0.1463414634
NN	3.37E-006	0.0443	0.317	0.323	0.1524390244
QP	6.20E-006	0.0768	0.459	0.323	0.1585365854
OG	4.47E-006	0.0634	0.155	0.335	0.1646341463
D	2.57E-006	0.0658	0.168	0.36	0.1707317073
PK	7.59E-006	0.0553	0.34	0.417	0.1768292683
OY	4.44E-006	0.0434	0.096	0.455	0.1829268293
PA	-3.34E-006	0.0292	0.295	0.457	0.1890243902
A	-9.22E-006	0.0666	0.0689	0.464	0.1951219512
OW	3.47E-006	0.0576	0.0942	0.554	0.2012195122
OZ	-2.97E-006	0.0559	0.0659	0.579	0.2073170732
OU	2.72E-006	0.0547	0.0508	0.592	0.2134146341
F	4.60E-006	0.0545	0.0488	0.634	0.2195121951
OE	5.77E-006	0.0432	0.0713	0.664	0.2256097561
OS	1.62E-006	0.0716	0.0361	0.683	0.2317073171
O1	1.84E-006	0.0657	0.0609	0.689	0.237804878
QD	2.38E-007	0.0551	0.0564	0.763	0.243902439

Chapter 5

Conclusions

It was unclear if, cross-sectionally derived HIV landscapes would concord well with HIV landscapes derived from longitudinal sequence data. With few exceptions (Seifert et al., 2015), most computationally derived fitness landscapes have been inferred using cross-sectionally sampled sequences. (Rihn et al., 2013; Mann et al., 2014; Ferguson et al., 2013; Barton et al., 2015). These models assume rank prevalence of strains is a sufficient indicator of fitness. However, there is evidence that these models sometimes fail to well predict spreading fitness and escape rate of viral mutants (Rihn et al., 2013; Liu et al., 2012; Barton et al., 2015). In our analysis, we discovered that estimates of fitness costs extracted from cross-sectional data did not well correlate with fitness costs extracted from longitudinal data. (Chapter 2 Fig 2.4). It appears that either 1) entropy/prevalence based methods are a poor proxy for fitness, 2) our method based on reversion rates is a poor proxy of fitness, or both fail to capture critical aspects of intra-host fitness.

We have developed a novel technique for constructing a one dimensional fitness landscape of HIV. This technique uses systems of differential equations to extract fitness landscape parameters from viral population dynamics. The resulting landscape denotes how costly it is for HIV to mutate single residues along its Gag protein (a common vaccine target Korber et al. (2009); Currier et al.

(2011)). We would like to extend this framework to examine double mutations along the HIV protein, as mutations tend to have strong interactions in HIV Bonhoeffer et al. (2004); Dahirel et al. (2011); Koek et al. (2012); Brockman et al. (2007). Often, amino acid mutations in combination will impact HIVs fitness differently than if they were to occur separately. These type of interactions are called epistatic interactions Silva et al. (2010). Two dimensional fitness maps accounting for epistatic interactions have been developed using cross-sectional database sequences Deforche et al. (2008); Seifert et al. (2015); Ferguson et al. (2013); Mann et al. (2014) and *in vitro* competitions assays Manocheewa et al. (2015); Hinkley et al. (2011); Lorenzo-Redondo et al. (2014). Our analysis, however, avoids the confounding problem of co-inheritance found in cross-sectional database methods Wang and Lee (2007). Also, unlike *in vitro* methods, this technique could describe how epistatic interactions as they occur in real patients. We could extend our single trajectory ODE model to fit double mutation trajectories. This will be accomplished by linking the fitness values of the two mutations in the current model so that they are simultaneously regarded as individual positions and as a mutating unit when a landscape parameter is extracted.

. As shown by (Zanini et al., 2016), when observing proxies for fitness cost the interior residues tend to much more costly to mutate compared with the exterior residues. This could very well explain the two grouped populations that emerge in both the shannon entropy metric and the sensitivity metric. One way in which we could verify that the grouping is arising due extremity or inferiority, is to map this information onto the metric using HXB2 coordinates for the virus and determine if this characteristic explains the grouping.

We als wished to determine if incorporating physico-chemical residue detail into a fitness landscape would improve its ability to predict and describe viral behaviors. We show in Chapter 3 that incorporating physico-chemical detail allowed us to better predict fitness spreading rates (Fig. 3.7) and escape times (Fig. 3.6). Shannon entropy is currently the metric of choice for predicting viral fitness behaviors, however, this metric has failed to always describe HIV fitness effects (Rihn et al., 2013; Liu et al., 2012; Barton et al., 2015). Others have inferred fitness landscapes ignore residue detail. As such, the resulting fitness maps cannot mechanistically describe the differential selective forces exerted on the residues (Barton et al., 2015; Mann et al., 2014). Alternatively, We have presented an approach for inferring fitness landscapes that possesses greater predictive power than shannon entropy and also allows us to pose biologically driven hypotheses about selection along the proteome (Fig 3.3).

Our physico-chemical framework allows us to appraise the descriptive power of various extensions and variations to the modeling schema in a statistically robust way. Four extensions and variations of the model that should be explored are as follows; **(1) Alternate Residue Characteristics** In the model the residue characteristic of composition, polarity, and molecular volume were regarded as the core principle characteristics determining residue interchangeability and fixation in HIV. However, we should determine if other sets of characteristics can appreciably improve the the model's explanatory power. Contending traits include continuous properties like hydrophobicity or acidity and categorical traits such as the aliphatic or aromatic side chain construction. **(2) Multiple Optimums** As mentioned previously, more than one physio-chemical optimum may exist for a position. The model can be adjusted to assess if adding this extra complexity for a position is justified. This added feature will help us avoid under-estimating sensitivity at positions where the optimum may shift. **(3) Variable Selection on Physico-Chemical Characteristics**. We have already demonstrated that certain characteristics are more critical to residue interchangeability in some regions rather than others. Given the selective forces are likely to be more consistent over structurally similar regions, sub-setting the selective weightings on these characteristics by secondary structures seems to be a logical way to improve the descriptive power of the model. **(4) Incorporating Epistasis** Finally, outside epistatic interactions between positions should be accounted for by extending our model to describe both single residue frequencies and paired residue frequencies. Landscapes that incorporate interactions between all positions can be computationally expensive to fit, so using a model selection framework to identify only those positions pairs that substantially improve the description of the multiple sequence alignment may be preferable.

Little is known about the fitness of HIV during acute infection (Arnott et al., 2010). However it is well established that HIV's structural elements are under both heavy purifying pressure and rapidly shed unfit polymorphims post transmission (Carlson et al., 2014; Novitsky et al., 2009). Given these observations, we might expect to see fitness increase over early infection as mutations accrued in the former patient are shed and the virus experiences an adaptive expansion post the transmission bottleneck. We concluded from analyzing longitudinal sampled virus, that HIV's structural proteins showed little to no discernible increase in fitness over early infection. Previously, an increase in overall viral replicative fitness over infection had been observed in 10 HIV-1 subtype B infected patients Troyer et al. (2005). It may be that *in vitro* fitness assays do not well mirror within host selective pressures for this poly-protein. Alternatively, overall viral fitness trends may not be reflective of the fitness trends of viral structural elements. In the future, it may pay to employ the physicochemical metric explored in Chapter 3 as a way to describe the structural protein's distance from the consensus strain.

Bibliography

2002. Basic Use of the Information-Theoretic Approach. In K. P. Burnham, and D. R. Anderson, eds., Model Selection and Multimodel Inference, pages 98–148. Springer New York. DOI: 10.1007/978-0-387-22456-5_3. 43

Abidi, S. H., M. L. Kalish, F. Abbas, S. Rowland-Jones, and S. Ali. 2014. HIV-1 Subtype A Gag Variability and Epitope Evolution. PLoS ONE 9:e93415. doi:10.1371/journal.pone.0093415. 76, 77

Acevedo, A., L. Brodsky, and R. Andino. 2014. Mutational and fitness landscapes of an RNA virus revealed through population sequencing. Nature 505:686–690. doi:10.1038/nature12861. 3, 4, 36

Agresti, A. 2003. Categorical Data Analysis. John Wiley & Sons. 68

Al-Mawsawi, L. Q., N. C. Wu, C. A. Olson, V. C. Shi, H. Qi, X. Zheng, T.-T. Wu, and R. Sun. 2014. High-throughput profiling of point mutations across the HIV-1 genome. Retrovirology 11:124. doi:10.1186/s12977-014-0124-6. 3, 4

Allen, T. M., M. Altfeld, S. C. Geer, E. T. Kalife, C. Moore, K. M. O'sullivan, I. Desouza, M. E. Feeney, R. L. Eldridge, E. L. Maier, D. E. Kaufmann, M. P. Lahaie, L. Reyor, G. Tanzi, M. N. Johnston, C. Brander, R. Draenert, J. K. Rockstroh, H. Jessen, E. S. Rosenberg, S. A. Mallal, and B. D. Walker. 2005. Selective escape from CD8+ T-cell responses represents a major driving force of human immunodeficiency virus type 1 (HIV-1) sequence diversity and reveals constraints on HIV-1 evolution. Journal of Virology 79:13239–13249. doi:10.1128/JVI.79.21.13239-13249.2005. 5

Arnott, A., D. Jardine, K. Wilson, P. R. Gorry, K. Merlin, P. Grey, M. G. Law, E. M. Dax, A. D. Kelleher, D. E. Smith, D. A. McPhee, and a. t. P. S. Team. 2010. High Viral Fitness during Acute HIV-1 Infection. PLOS ONE 5:e12631. doi:10.1371/journal.pone.0012631. 9, 62, 87

Autran, B., R. L. Murphy, D. Costagliola, R. Tubiana, B. Clotet, J. Gatell, S. Staszewski, N. Wincker, L. Assoumou, R. El-Habib, V. Calvez, B. Walker, C. Katlama, and ORVACS Study Group. 2008. Greater viral rebound and reduced time to resume antiretroviral therapy after therapeutic immunization with the ALVAC-HIV vaccine (vCP1452). AIDS (London, England) 22:1313–1322. doi:10.1097/QAD.0b013e3282fdce94. 36

Barton, J. P., M. Kardar, and A. K. Chakraborty. 2015. Scaling laws describe memories of host-pathogen riposte in the HIV population. Proceedings of the National Academy of Sciences of the United States of America 112:1965–1970. doi:10.1073/pnas.1415386112. 27, 84, 86

Barton, J. P., N. Goonetilleke, T. C. Butler, B. D. Walker, A. J. McMichael, and A. K. Chakraborty. 2016. Relative rate and location of intra-host HIV evolution to evade cellular immunity are predictable. Nature Communications 7:11660. doi:10.1038/ncomms11660. 1, 2, 5, 6, 7, 8, 36

Bonhoeffer, S., C. Chappey, N. T. Parkin, J. M. Whitcomb, and C. J. Petropoulos. 2004. Evidence for positive epistasis in HIV-1. Science (New York, N.Y.) 306:1547–1550. doi:10.1126/science.1101786. 85

Borrow, P., H. Lewicki, B. H. Hahn, G. M. Shaw, and M. B. Oldstone. 1994. Virus-specific CD8+ cytotoxic T-lymphocyte activity associated with control of viremia in primary human immunodeficiency virus type 1 infection. Journal of Virology 68:6103–6110. 28

Brockman, M. A., A. Schneidewind, M. Lahaie, A. Schmidt, T. Miura, I. Desouza, F. Ryvkin, C. A. Derdeyn, S. Allen, E. Hunter, J. Mulenga, P. A. Goepfert, B. D. Walker, and T. M. Allen. 2007. Escape and Compensation from Early HLA-B57-Mediated Cytotoxic T-Lymphocyte Pressure on Human Immunodeficiency Virus Type 1 Gag Alter Capsid Interactions with Cyclophilin A. Journal of Virology 81:12608–12618. doi:10.1128/JVI.01369-07. 28, 64, 85

Brockman, M. A., Z. L. Brumme, C. J. Brumme, T. Miura, J. Sela, P. C. Rosato, C. M. Kadie, J. M. Carlson, T. J. Markle, H. Streeck, A. D. Kelleher, M. Markowitz, H. Jessen, E. Rosenberg, M. Altfeld, P. R. Harrigan, D. Heckerman, B. D. Walker, and T. M. Allen. 2010. Early Selection in Gag by Protective HLA Alleles Contributes to Reduced HIV-1 Replication Capacity That May Be Largely Compensated for in Chronic Infection. Journal of Virology 84:11937–11949. doi:10.1128/JVI.01086-10. 64

Brown, L. D., T. T. Cai, and A. DasGupta. 2001. Interval Estimation for a Binomial Proportion. Statistical Science 16:101–117. ArticleType: research-article / Full publication date: May, 2001 / Copyright 2001 Institute of Mathematical Statistics. 15, 16

Burwitz, B. J., J. B. Sacha, J. S. Reed, L. P. Newman, F. A. Norante, B. N. Bimber, N. A. Wilson, D. I. Watkins, and D. H. O'Connor. 2011. Pyrosequencing Reveals Restricted Patterns of CD8+ T Cell Escape-Associated Compensatory Mutations in Simian Immunodeficiency Virus. Journal of Virology 85:13088–13096. doi:10.1128/JVI.05650-11. 64, 77

Carlson, J. M., M. Schaefer, D. C. Monaco, R. Batorsky, D. T. Claiborne, J. Prince, M. J. Deymier, Z. S. Ende, N. R. Klatt, C. E. DeZiel, T.-H. Lin, J. Peng, A. M. Seese, R. Shapiro, J. Frater, T. Ndungu, J. Tang, P. Goepfert, J. Gilmour, M. A. Price, W. Kilembe, D. Heckerman, P. J. R. Goulder, T. M. Allen, S. Allen, and E. Hunter. 2014. Selection bias at the heterosexual HIV-1 transmission bottleneck. Science 345:1254031. doi:10.1126/science.1254031. 62, 63, 87

Chopera, D. R., J. K. Wright, M. A. Brockman, and Z. L. Brumme. 2011. Immune-mediated attenuation of HIV-1. Future Virology 6:917–928. doi:10.2217/fvl.11.68. 2

Croux, C., and C. Dehon. 2010. Influence functions of the Spearman and Kendall correlation measures. Statistical Methods & Applications 19:497–515. doi:10.1007/s10260-010-0142-z. 42

Cuevas, J. M., R. Geller, R. Garijo, J. Lpez-Aldeguer, and R. Sanjun. 2015. Extremely High Mutation Rate of HIV-1 In Vivo. PLoS Biology 13. doi:10.1371/journal.pbio.1002251. 27, 36

Currier, J. R., M. L. Robb, N. L. Michael, and M. A. Marovich. 2011. Defining epitope coverage requirements for T cell-based HIV vaccines: Theoretical considerations and practical applications. Journal of Translational Medicine 9:212. doi:10.1186/1479-5876-9-212. 84

Dahirel, V., K. Shekhar, F. Pereyra, T. Miura, M. Artyomov, S. Talsania, T. M. Allen, M. Altfeld, M. Carrington, D. J. Irvine, B. D. Walker, and A. K. Chakraborty. 2011. Coordinate linkage of HIV evolution reveals regions of immunological vulnerability. Proceedings of the National Academy of Sciences doi:10.1073/pnas.1105315108. 6, 28, 64, 77, 85

Davenport, M. P., L. Loh, J. Petravic, and S. J. Kent. 2008. Rates of HIV immune escape and reversion: implications for vaccination. Trends in Microbiology 16:561–566. doi:10.1016/j.tim.2008.09.001. 13

Deforche, K., R. Camacho, K. V. Laethem, P. Lemey, A. Rambaut, Y. Moreau, and A.-M. Vandamme. 2008. Estimation of an in vivo fitness landscape experienced by HIV-1 under drug selective pressure useful for prediction of drug resistance evolution during treatment. Bioinformatics 24:34–41. doi:10.1093/bioinformatics/btm540. 36, 85

Ferguson, A. L., J. K. Mann, S. Omarjee, T. Ndungu, B. D. Walker, and A. K. Chakraborty. 2013. Translating HIV sequences into quantitative fitness landscapes predicts viral vulnerabilities for rational immunogen design. Immunity 38:606–617. doi:10.1016/j.immuni.2012.11.022. 1, 2, 6, 7, 8, 12, 18, 28, 36, 65, 84, 85

Fernandes, J. D., T. B. Faust, N. B. Strauli, C. Smith, D. C. Crosby, R. L. Nakamura, R. D. Hernandez, and A. D. Frankel. 2016. Functional Segregation of Overlapping Genes in HIV. Cell 167:1762–1773.e12. doi:10.1016/j.cell.2016.11.031. 5

Fernandez, C. S., I. Stratov, R. D. Rose, K. Walsh, C. J. Dale, M. Z. Smith, M. B. Agy, S.-I. Hu, K. Krebs, D. I. Watkins, D. H. O'Connor, M. P. Davenport, and S. J. Kent. 2005. Rapid Viral Escape at an Immunodominant Simian-Human Immunodeficiency Virus Cytotoxic T-Lymphocyte Epitope Exacts a Dramatic Fitness Cost. Journal of Virology 79:5721–5731. doi:10.1128/JVI.79.9.5721-5731.2005. 13

Ferrari, G., B. Korber, N. Goonetilleke, M. K. P. Liu, E. L. Turnbull, J. F. Salazar-Gonzalez, N. Hawkins, S. Self, S. Watson, M. R. Betts, C. Gay, K. McGhee, P. Pellegrino, I. Williams, G. D. Tomaras, B. F. Haynes, C. M. Gray, P. Borrow, M. Roederer, A. J. McMichael, and K. J. Weinhold. 2011. Relationship between Functional Profile of HIV-1 Specific CD8 T Cells and Epitope Variability with the Selection of Escape Mutants in Acute HIV-1 Infection. PLOS Pathog 7:e1001273. doi:10.1371/journal.ppat.1001273. 1, 5, 12, 43

Folkvord, J. M., C. Armon, and E. Connick. 2005. Lymphoid follicles are sites of heightened human immunodeficiency virus type 1 (HIV-1) replication and reduced antiretroviral effector mechanisms. AIDS research and human retroviruses 21:363–370. doi:10.1089/aid.2005.21.363. 27

Ganusov, V. V., and R. J. De Boer. 2006. Estimating Costs and Benefits of CTL Escape Mutations in SIV/HIV Infection. PLoS Comput Biol 2:e24. doi:10.1371/journal.pcbi.0020024. 13

GARPR. 2016. Global AIDS Update 2016. 12

Geller, R., P. Domingo-Calap, J. M. Cuevas, P. Rossolillo, M. Negroni, and R. Sanjun. 2015. The external domains of the HIV-1 envelope are a mutational cold spot. Nature Communications 6:8571. doi:10.1038/ncomms9571. 27

Gilchrist, M. A. 2007. Combining Models of Protein Translation and Population Genetics to Predict Protein Production Rates from Codon Usage Patterns. Molecular Biology and Evolution 24:2362–2372. doi:10.1093/molbev/msm169. 14, 36

Gilchrist, M. A., P. Shah, and R. Zaretzki. 2009. Measuring and Detecting Molecular Adaptation in Codon Usage Against Nonsense Errors During Protein Translation. Genetics 183:1493–1505. doi:10.1534/genetics.109.108209. 14, 36

Goulder, P. J. R., and D. I. Watkins. 2004. HIV and SIV CTL escape: implications for vaccine design. Nature Reviews Immunology 4:630–640. doi:10.1038/nri1417. 36, 63

Grantham, R. 1974. Amino acid difference formula to help explain protein evolution. Science (New York, N.Y.) 185:862–864. 13, 14, 37, 38, 41, 44

Heath, L., A. Fox, J. McClure, K. Diem, A. B. v. t. Wout, H. Zhao, D. R. Park, J. T. Schouten, H. L. T. Iii, L. Corey, J. I. Mullins, and J. E. Mittler. 2009. Evidence for Limited Genetic Compartmentalization of HIV-1 between Lung and Blood. PLOS ONE 4:e6949. doi:10.1371/journal.pone.0006949. 27

Hedskog, C., M. Mild, J. Jernberg, E. Sherwood, G. Bratt, T. Leitner, J. Lundeberg, B. Andersson, and J. Albert. 2010. Dynamics of HIV-1 Quasispecies during Antiviral Treatment Dissected Using Ultra-Deep Pyrosequencing. PLoS ONE 5:e11345. doi:10.1371/journal.pone.0011345. 13

Hinkley, T., J. Martins, C. Chappey, M. Haddad, E. Stawiski, J. M. Whitcomb, C. J. Petropoulos, and S. Bonhoeffer. 2011. A systems analysis of mutational effects in HIV-1 protease and reverse transcriptase. Nature Genetics 43:487–489. doi:10.1038/ng.795. 3, 4, 36, 85

Holland, J. J., J. C. d. l. Torre, D. K. Clarke, and E. Duarte. 1991. Quantitation of relative fitness and great adaptability of clonal populations of RNA viruses. Journal of Virology 65:2960–2967. 3

Holmes, E. C., and A. Moya. 2002. Is the Quasispecies Concept Relevant to RNA Viruses? Journal of Virology 76:460–462. doi:10.1128/JVI.76.1.460-462.2002. 13

Honeyborne, I., A. Prendergast, F. Pereyra, A. Leslie, H. Crawford, R. Payne, S. Reddy, K. Bishop, E. Moodley, K. Nair, M. van der Stok, N. McCarthy, C. M. Rousseau, M. Addo, J. I. Mullins, C. Brander, P. Kiepiela, B. D. Walker, and P. J. R. Goulder. 2007. Control of Human Immunodeficiency Virus Type 1 Is Associated with HLA-B*13 and Targeting of Multiple Gag-Specific CD8+ T-Cell Epitopes. Journal of Virology 81:3667–3672. doi:10.1128/JVI.02689-06. 63

Hufert, F. T., J. van Lunzen, G. Janossy, S. Bertram, J. Schmitz, O. Haller, P. Racz, and D. von Laer. 1997. Germinal centre CD4+ T cells are an important site of HIV replication in vivo. AIDS (London, England) 11:849–857. 27

Jeffreys, H. 1946. An Invariant Form for the Prior Probability in Estimation Problems. Proceedings of the Royal Society of London A: Mathematical, Physical and Engineering Sciences 186:453–461. doi:10.1098/rspa.1946.0056. 15

Johnston, M. I., and A. S. Fauci. 2008. An HIV Vaccine Challenges and Prospects. New England Journal of Medicine 359:888–890. doi:10.1056/NEJMp0806162. 1, 36

Kendall, M. G., and J. D. Gibbons. 1990. Rank correlation methods. E. Arnold. Google-Books-ID: ly4nAQAAIAAJ. 42

Kim, E.-Y., R. Lorenzo-Redondo, S. J. Little, Y.-S. Chung, P. K. Phalora, I. Maljkovic Berry, J. Archer, S. Penugonda, W. Fischer, D. D. Richman, T. Bhattacharya, M. H. Malim, and S. M. Wolinsky. 2014. Human APOBEC3 Induced Mutation of Human Immunodeficiency Virus Type-1 Contributes to Adaptation and Evolution in Natural Infection. PLoS Pathogens 10. doi:10.1371/journal.ppat.1004281. 27

Korber, B., B. Gaschen, K. Yusim, R. Thakallapally, C. Kesmir, and V. Detours. 2001. Evolutionary and immunological implications of contemporary HIV-1 variation. British Medical Bulletin 58:19–42. 1, 36, 78

Korber, B. T., N. L. Letvin, and B. F. Haynes. 2009. T-Cell Vaccine Strategies for Human Immunodeficiency Virus, the Virus with a Thousand Faces. Journal of Virology 83:8300–8314. doi:10.1128/JVI.00114-09. 63, 77, 84

Kouyos, R. D., G. E. Leventhal, T. Hinkley, M. Haddad, J. M. Whitcomb, C. J. Petropoulos, and S. Bonhoeffer. 2012. Exploring the Complexity of the HIV-1 Fitness Landscape. PLoS Genet 8:e1002551. doi:10.1371/journal.pgen.1002551. 36

Koek, M., S. Henke, K. G. akov, G. B. Jacobs, A. Schuch, B. Buchholz, V. Mller, H.-G. Krusslich, P. ezov, J. Konvalinka, and J. Bodem. 2012. Mutations in HIV-1 gag and pol Compensate for the Loss of Viral Fitness Caused by a Highly Mutated Protease. Antimicrobial Agents and Chemotherapy 56:4320–4330. doi:10.1128/AAC.00465-12. 77, 85

Lemey, P., A. Rambaut, and O. G. Pybus. 2006. HIV evolutionary dynamics within and among hosts. AIDS reviews 8:125–140. 36

Li, B., A. D. Gladden, M. Altfeld, J. M. Kaldor, D. A. Cooper, A. D. Kelleher, and T. M. Allen. 2007. Rapid Reversion of Sequence Polymorphisms Dominates Early Human Immunodeficiency Virus Type 1 Evolution. Journal of Virology 81:193–201. doi:10.1128/JVI.01231-06. 5, 63, 77

Li, G., J. Verheyen, S.-Y. Rhee, A. Voet, A.-M. Vandamme, and K. Theys. 2013. Functional conservation of HIV-1 Gag: implications for rational drug design. Retrovirology 10:126. doi:10.1186/1742-4690-10-126. 9

Li, H., K. J. Bar, S. Wang, J. M. Decker, Y. Chen, C. Sun, J. F. Salazar-Gonzalez, M. G. Salazar, G. H. Learn, C. J. Morgan, J. E. Schumacher, P. Hraber, E. E. Giorgi, T. Bhattacharya, B. T.

Korber, A. S. Perelson, J. J. Eron, M. S. Cohen, C. B. Hicks, B. F. Haynes, M. Markowitz, B. F. Keele, B. H. Hahn, and G. M. Shaw. 2010. High Multiplicity Infection by HIV-1 in Men Who Have Sex with Men. PLoS Pathog 6:e1000890. doi:10.1371/journal.ppat.1000890. 63

Liu, M. K., N. Hawkins, A. J. Ritchie, V. V. Ganusov, V. Whale, S. Brackenridge, H. Li, J. W. Pavlicek, F. Cai, M. Rose-Abrahams, F. Treurnicht, P. Hraber, C. Riou, C. Gray, G. Ferrari, R. Tanner, L.-H. Ping, J. A. Anderson, R. Swanstrom, C. C. B, M. Cohen, S. S. A. Karim, B. Haynes, P. Borrow, A. S. Perelson, G. M. Shaw, B. H. Hahn, C. Williamson, B. T. Korber, F. Gao, S. Self, A. McMichael, and N. Goonetilleke. 2012. Vertical T cell immunodominance and epitope entropy determine HIV-1 escape. Journal of Clinical Investigation doi:10.1172/JCI65330. 1, 2, 3, 5, 12, 28, 43, 84, 86

Lorenzo-Redondo, R., S. Delgado, F. Morn, and C. Lopez-Galindez. 2014. Realistic Three Dimensional Fitness Landscapes Generated by Self Organizing Maps for the Analysis of Experimental HIV-1 Evolution. PLoS ONE 9:e88579. doi:10.1371/journal.pone.0088579. 36, 85

Mann, J. K., J. P. Barton, A. L. Ferguson, S. Omarjee, B. D. Walker, A. Chakraborty, and T. Ndung'u. 2014. The Fitness Landscape of HIV-1 Gag: Advanced Modeling Approaches and Validation of Model Predictions by In Vitro Testing. PLoS Comput Biol 10:e1003776. doi:10.1371/journal.pcbi.1003776. 1, 2, 6, 7, 8, 12, 18, 36, 84, 85, 86

Manocheewa, S., E. C. Lanxon-Cookson, Y. Liu, J. V. Swain, J. McClure, U. Rao, B. Maust, W. Deng, J. E. Sunshine, M. Kim, M. Rolland, and J. I. Mullins. 2015. Pairwise Growth Competition Assay for Determining the Replication Fitness of Human Immunodeficiency Viruses. Journal of Visualized Experiments : JoVE doi:10.3791/52610. 3, 36, 85

Martinez-Picado, J., J. G. Prado, E. E. Fry, K. Pfafferott, A. Leslie, S. Chetty, C. Thobakgale, I. Honeyborne, H. Crawford, P. Matthews, T. Pillay, C. Rousseau, J. I. Mullins, C. Brander,

B. D. Walker, D. I. Stuart, P. Kiepiela, and P. Goulder. 2006. Fitness cost of escape mutations in p24 Gag in association with control of human immunodeficiency virus type 1. Journal of virology 80:3617–3623. doi:10.1128/JVI.80.7.3617-3623.2006. 36

McElrath, M. J., and B. F. Haynes. 2010. Induction of immunity to human immunodeficiency virus type-1 by vaccination. Immunity 33:542–554. doi:10.1016/j.immuni.2010.09.011. 1

Michael R. Dietrich, R. S. 2012. A Shifting Terrain: A Brief History of the Adaptive Landscape. The adaptive landscape in evolutionary biology pages 3–15. 36

Miura, T., Z. L. Brumme, M. A. Brockman, P. Rosato, J. Sela, C. J. Brumme, F. Pereyra, D. E. Kaufmann, A. Trocha, B. L. Block, E. S. Daar, E. Connick, H. Jessen, A. D. Kelleher, E. Rosenberg, M. Markowitz, K. Schafer, F. Vaida, A. Iwamoto, S. Little, and B. D. Walker. 2010. Impaired Replication Capacity of Acute/Early Viruses in Persons Who Become HIV Controllers. Journal of Virology 84:7581–7591. doi:10.1128/JVI.00286-10. 12, 62

Moradigaravand, D., R. Kouyos, T. Hinkley, M. Haddad, C. J. Petropoulos, J. Engelstdter, and S. Bonhoeffer. 2014. Recombination Accelerates Adaptation on a Large-Scale Empirical Fitness Landscape in HIV-1. PLoS Genet 10:e1004439. doi:10.1371/journal.pgen.1004439. 36

Novitsky, V., R. Wang, L. Margolin, J. Baca, L. Kebaabetswe, R. Rossenkhan, C. Bonney, M. Herzig, D. Nkwe, S. Moyo, R. Musonda, E. Woldegabriel, E. van Widenfelt, J. Makhema, S. Lagakos, and M. Essex. 2009. Timing Constraints of In Vivo Gag Mutations during Primary HIV-1 Subtype C Infection. PLoS ONE 4:e7727. doi:10.1371/journal.pone.0007727. 8, 9, 15, 28, 62, 64, 72, 87

Novitsky, V., R. Wang, J. Baca, L. Margolin, M. F. McLane, S. Moyo, E. van Widenfelt, J. Makhema, and M. Essex. 2011. Evolutionary Gamut of in vivo Gag Substitutions during Early HIV-1 Subtype C Infection. Virology 421:119–128. doi:10.1016/j.virol.2011.09.020. 22, 29, 64

Novitsky, V., R. Wang, R. Rossenkhan, S. Moyo, and M. Essex. 2013. Intra-host evolutionary rates in HIV-1c env and gag during primary infection. Infection, Genetics and Evolution 19:361–368. doi:10.1016/j.meegid.2013.02.023. 62, 77

Ogg, G. S., X. Jin, S. Bonhoeffer, P. R. Dunbar, M. A. Nowak, S. Monard, J. P. Segal, Y. Cao, S. L. Rowland-Jones, V. Cerundolo, A. Hurley, M. Markowitz, D. D. Ho, D. F. Nixon, and A. J. McMichael. 1998. Quantitation of HIV-1-specific cytotoxic T lymphocytes and plasma load of viral RNA. Science (New York, N.Y.) 279:2103–2106. 28

Parera, M., G. Fernndez, B. Clotet, and M. A. Martnez. 2007. HIV-1 Protease Catalytic Efficiency Effects Caused by Random Single Amino Acid Substitutions. Molecular Biology and Evolution 24:382–387. doi:10.1093/molbev/msl168. 4

Pennings, P. S., S. Kryazhimskiy, and J. Wakeley. 2014. Loss and Recovery of Genetic Diversity in Adapting Populations of HIV. PLoS Genet 10:e1004000. doi:10.1371/journal.pgen.1004000. 78

Petropoulos, C. J., N. T. Parkin, K. L. Limoli, Y. S. Lie, T. Wrin, W. Huang, H. Tian, D. Smith, G. A. Winslow, D. J. Capon, and J. M. Whitcomb. 2000. A Novel Phenotypic Drug Susceptibility Assay for Human Immunodeficiency Virus Type 1. Antimicrobial Agents and Chemotherapy 44:920–928. doi:10.1128/AAC.44.4.920-928.2000. 4

Pilcher, C. D., J. K. Wong, and S. K. Pillai. 2008. Inferring HIV Transmission Dynamics from Phylogenetic Sequence Relationships. PLoS Medicine 5. doi:10.1371/journal.pmed.0050069. 65

Quiones-Mateu, M. E., S. C. Ball, A. J. Marozsan, V. S. Torre, J. L. Albright, G. Vanham, G. v. d. Groen, R. L. Colebunders, and E. J. Arts. 2000. A Dual Infection/Competition Assay Shows a Correlation between Ex Vivo Human Immunodeficiency Virus Type 1 Fitness and Disease

Progression. Journal of Virology 74:9222–9233. doi:10.1128/JVI.74.19.9222-9233.2000. 9, 63

Rihn, S. J., S. J. Wilson, N. J. Loman, M. Alim, S. E. Bakker, D. Bhella, R. J. Gifford, F. J. Rixon, and P. D. Bieniasz. 2013. Extreme Genetic Fragility of the HIV-1 Capsid. PLoS Pathog 9:e1003461. doi:10.1371/journal.ppat.1003461. 1, 2, 3, 4, 5, 12, 27, 36, 43, 55, 62, 76, 77, 84, 86

Rolland, M., D. Heckerman, W. Deng, C. M. Rousseau, H. Coovadia, K. Bishop, P. J. R. Goulder, B. D. Walker, C. Brander, and J. I. Mullins. 2008. Broad and Gag-Biased HIV-1 Epitope Repertoires Are Associated with Lower Viral Loads. PLOS ONE 3:e1424. doi:10.1371/journal.pone.0001424. 63

Rolland, M., J. M. Carlson, S. Manocheewa, J. V. Swain, E. Lanxon-Cookson, W. Deng, C. M. Rousseau, D. N. Raugi, G. H. Learn, B. S. Maust, H. Coovadia, T. Ndung'u, P. J. R. Goulder, B. D. Walker, C. Brander, D. E. Heckerman, and J. I. Mullins. 2010. Amino-Acid Co-Variation in HIV-1 Gag Subtype C: HLA-Mediated Selection Pressure and Compensatory Dynamics. PLoS ONE 5. doi:10.1371/journal.pone.0012463. 77

Rouzine, I. M., and L. S. Weinberger. 2013. The quantitative theory of within-host viral evolution. Journal of Statistical Mechanics: Theory and Experiment 2013:P01009. 13

Rozera, G., I. Abbate, C. Vlassi, E. Giombini, R. Lionetti, M. Selleri, P. Zaccaro, B. Bartolini, A. Corpolongo, G. D'Offizi, A. Baiocchini, F. Del Nonno, G. Ippolito, and M. R. Capobianchi. 2014. Quasispecies tropism and compartmentalization in gut and peripheral blood during early and chronic phases of HIV-1 infection: possible correlation with immune activation markers. Clinical Microbiology and Infection 20:O157–O166. doi:10.1111/1469-0691.12367. 13, 27

Salemi, M. 2013. The Intra-Host Evolutionary and Population Dynamics of Human Immunodeficiency Virus Type 1: A Phylogenetic Perspective. Infectious Disease Reports 5. doi:10.4081/idr.2013.s1.e3. 36

Sanjun, R., M. R. Nebot, N. Chirico, L. M. Mansky, and R. Belshaw. 2010. Viral Mutation Rates. Journal of Virology 84:9733–9748. doi:10.1128/JVI.00694-10. 1

Schacker, T. 2008. The role of secondary lymphatic tissue in immune deficiency of HIV infection. AIDS (London, England) 22 Suppl 3:S13–18. doi:10.1097/01.aids.0000327511.76126.b5. 27

Schneidewind, A., M. A. Brockman, R. Yang, R. I. Adam, B. Li, S. Le Gall, C. R. Rinaldo, S. L. Craggs, R. L. Allgaier, K. A. Power, T. Kuntzen, C.-S. Tung, M. X. LaBute, S. M. Mueller, T. Harrer, A. J. McMichael, P. J. R. Goulder, C. Aiken, C. Brander, A. D. Kelleher, and T. M. Allen. 2007. Escape from the dominant HLA-B27-restricted cytotoxic T-lymphocyte response in Gag is associated with a dramatic reduction in human immunodeficiency virus type 1 replication. Journal of Virology 81:12382–12393. doi:10.1128/JVI.01543-07. 28

Seifert, D., F. D. Giallonardo, K. J. Metzner, H. F. Gnthard, and N. Beerenwinkel. 2015. A Framework for Inferring Fitness Landscapes of Patient-Derived Viruses Using Quasispecies Theory. Genetics 199:191–203. doi:10.1534/genetics.114.172312. 36, 84, 85

Sella, G., and A. E. Hirsh. 2005. The application of statistical physics to evolutionary biology. Proceedings of the National Academy of Sciences of the United States of America 102:9541–9546. doi:10.1073/pnas.0501865102. 37, 39

Shah, P., and M. A. Gilchrist. 2011. Explaining complex codon usage patterns with selection for translational efficiency, mutation bias, and genetic drift. Proceedings of the National Academy of Sciences 108:10231–10236. doi:10.1073/pnas.1016719108. 14, 36

Shekhar, K., C. F. Ruberman, A. L. Ferguson, J. P. Barton, M. Kardar, and A. K. Chakraborty. 2013. Spin models inferred from patient-derived viral sequence data faithfully describe HIV fitness landscapes. Physical Review. E, Statistical, Nonlinear, and Soft Matter Physics 88:062705. doi:10.1103/PhysRevE.88.062705. 2, 7, 12, 13, 18, 36

Shriner, D., R. Shankarappa, M. A. Jensen, D. C. Nickle, J. E. Mittler, J. B. Margolick, and J. I. Mullins. 2004. Influence of Random Genetic Drift on Human Immunodeficiency Virus Type 1 env Evolution During Chronic Infection. Genetics 166:1155–1164. doi:10.1534/genetics.166.3.1155. 13

Silva, J. d., M. Coetzer, R. Nedellec, C. Pastore, and D. E. Mosier. 2010. Fitness Epistasis and Constraints on Adaptation in a Human Immunodeficiency Virus Type 1 Protein Region. Genetics 185:293–303. doi:10.1534/genetics.109.112458. 85

Sturdevant, C. B., S. B. Joseph, G. Schnell, R. W. Price, R. Swanstrom, and S. Spudich. 2015. Compartmentalized Replication of R5 T Cell-Tropic HIV-1 in the Central Nervous System Early in the Course of Infection. PLOS Pathogens 11:e1004720. doi:10.1371/journal.ppat.1004720. 13, 27

Sunshine, J. E., B. B. Larsen, B. Maust, E. Casey, W. Deng, L. Chen, D. H. Westfall, M. Kim, H. Zhao, S. Ghorai, E. Lanxon-Cookson, M. Rolland, A. C. Collier, J. Maenza, J. I. Mullins, and N. Frahm. 2015. Fitness-Balanced Escape Determines Resolution of Dynamic Founder Virus Escape Processes in HIV-1 Infection. Journal of Virology 89:10303–10318. doi:10.1128/JVI.01876-15. 12

Thyagarajan, B., and J. D. Bloom. 2014. The inherent mutational tolerance and antigenic evolvability of influenza hemagglutinin. eLife 3:e03300. doi:10.7554/eLife.03300. 3, 4, 5

Tripathi, K., R. Balagam, N. K. Vishnoi, and N. M. Dixit. 2012. Stochastic Simulations Suggest that HIV-1 Survives Close to Its Error Threshold. PLoS Computational Biology 8. doi:10.1371/journal.pcbi.1002684. 63

Troyer, R. M., K. R. Collins, A. Abraha, E. Fraundorf, D. M. Moore, R. W. Krizan, Z. Toossi, R. L. Colebunders, M. A. Jensen, J. I. Mullins, G. Vanham, and E. J. Arts. 2005. Changes in Human Immunodeficiency Virus Type 1 Fitness and Genetic Diversity during Disease Progression. Journal of Virology 79:9006–9018. doi:10.1128/JVI.79.14.9006-9018.2005. 9, 62, 63, 76, 87

Troyer, R. M., J. McNevin, Y. Liu, S. C. Zhang, R. W. Krizan, A. Abraha, D. M. Tebit, H. Zhao, S. Avila, M. A. Lobritz, M. J. McElrath, S. Le Gall, J. I. Mullins, and E. J. Arts. 2009. Variable Fitness Impact of HIV-1 Escape Mutations to Cytotoxic T Lymphocyte (CTL) Response. PLoS Pathog 5:e1000365. doi:10.1371/journal.ppat.1000365. 12

Tsibris, A. M. N., B. Korber, R. Arnaout, C. Russ, C.-C. Lo, T. Leitner, B. Gaschen, J. Theiler, R. Paredes, Z. Su, M. D. Hughes, R. M. Gulick, W. Greaves, E. Coakley, C. Flexner, C. Nusbaum, and D. R. Kuritzkes. 2009. Quantitative Deep Sequencing Reveals Dynamic HIV-1 Escape and Large Population Shifts during CCR5 Antagonist Therapy In Vivo. PLoS ONE 4:e5683. doi:10.1371/journal.pone.0005683. 13

van Marle, G., M. J. Gill, D. Kolodka, L. McManus, T. Grant, and D. L. Church. 2007. Compartmentalization of the gut viral reservoir in HIV-1 infected patients. Retrovirology 4:87. doi:10.1186/1742-4690-4-87. 13, 27

Waheed, A. A., and E. O. Freed. 2012. HIV Type 1 Gag as a Target for Antiviral Therapy. AIDS Research and Human Retroviruses 28:54–75. doi:10.1089/aid.2011.0230. 63

Walker, B. D., and D. R. Burton. 2008. Toward an AIDS Vaccine. Science 320:760–764. doi:10.1126/science.1152622. 1, 12, 77

Wang, Q., and C. Lee. 2007. Distinguishing Functional Amino Acid Covariation from Background Linkage Disequilibrium in HIV Protease and Reverse Transcriptase. PLoS ONE 2. doi:10.1371/journal.pone.0000814. 85

Wood, N., T. Bhattacharya, B. F. Keele, E. Giorgi, M. Liu, B. Gaschen, M. Daniels, G. Ferrari, B. F. Haynes, A. McMichael, G. M. Shaw, B. H. Hahn, B. Korber, and C. Seoighe. 2009. HIV Evolution in Early Infection: Selection Pressures, Patterns of Insertion and Deletion, and the Impact of APOBEC. PLOS Pathogens 5:e1000414. doi:10.1371/journal.ppat.1000414. 27

Wright, S. 1932. The roles of mutation, inbreeding, crossbreeding and selection in evolution. Proceedings of the sixth international congress of genetics 6:356–366. 1

Wu, N. C., A. P. Young, L. Q. Al-Mawsawi, C. A. Olson, J. Feng, H. Qi, S.-H. Chen, I.-H. Lu, C.-Y. Lin, R. G. Chin, H. H. Luan, N. Nguyen, S. F. Nelson, X. Li, T.-T. Wu, and R. Sun. 2014. High-throughput profiling of influenza A virus hemagglutinin gene at single-nucleotide resolution. Scientific Reports 4:4942. doi:10.1038/srep04942. 3, 4, 5

Zanini, F., V. Puller, J. Brodin, J. Albert, and R. Neher. 2016. In-vivo mutation rates and fitness landscape of HIV-1. bioRxiv page 045039. doi:10.1101/045039. 1, 3, 5, 6, 7, 8, 85

Vita

Elizabeth Johnson was born in Pittsfield, MA in 1986. In 2002 she was admitted to Appalachian State University as a Chancellor Scholar where she graduated *summa cum laude* in 2006 with a Bachelors of Science in Biology and minors in both Mathematics and Chemistry. She accepted a graduate position at the University of Tennessee Knoxville in 2010, where she was funded by an NSF Graduate Education and Research Fellowship for Scalable Computing in Biology and an assistantship from the National Institute for Mathematical and Biological Synthesis (NIMBioS). She pursued a doctorate under Vitaly Ganusov in a theoretical immunology laboratory housed in the Microbiology Department. There, she completed her computational minor and dissertation research on HIV fitness landscapes.